ISSN 1949-8470 (online)

World Journal of *Radiology*

World J Radiol 2024 January 28; 16(1): 1-31

Published by Baishideng Publishing Group Inc

World Journal of Radiology

Contents

Monthly Volume 16 Number 1 January 28, 2024

World Journal of Radiology

Monthly Volume 16 Number 1 January 28, 2024

Contents

ABOUT COVER

Associate Editor of *World Journal of Radiology*, Matteo Bauckneht, MD, PhD, Assistant Professor, Department of Health Sciences, University of Genova and IRCCS Ospedale Policlinico San Martino, Genova 16132, Italy. matteo.bauckneht@hsanmartino.it

AIMS AND SCOPE

The primary aim of *World Journal of Radiology* (*WJR*, *World J Radiol*) is to provide scholars and readers from various fields of radiology with a platform to publish high-quality basic and clinical research articles and communicate their research findings online.

WJR mainly publishes articles reporting research results and findings obtained in the field of radiology and covering a wide range of topics including state of the art information on cardiopulmonary imaging, gastrointestinal imaging, genitourinary imaging, musculoskeletal imaging, neuroradiology/head and neck imaging, nuclear medicine and molecular imaging, pediatric imaging, vascular and interventional radiology, and women's imaging.

INDEXING/ABSTRACTING

The *WJR* is now abstracted and indexed in PubMed, PubMed Central, Emerging Sources Citation Index (Web of Science), Reference Citation Analysis, China Science and Technology Journal Database, and Superstar Journals Database. The 2023 Edition of Journal Citation Reports® cites the 2022 impact factor (IF) for *WJR* as 2.5; IF without journal self cites: 2.3; 5-year IF: 2.5; Journal Citation Indicator: 0.54.

RESPONSIBLE EDITORS FOR THIS ISSUE

NAME OF JOURNAL
World Journal of Radiology

ISSN
ISSN 1949-8470 (online)

LAUNCH DATE
January 31, 2009

FREQUENCY
Monthly

EDITORS-IN-CHIEF
Thomas J Vogl

EDITORIAL BOARD MEMBERS
https://www.wjgnet.com/1949-8470/editorialboard.htm

PUBLICATION DATE
January 28, 2024

INSTRUCTIONS TO AUTHORS
https://www.wjgnet.com/bpg/gerinfo/204

GUIDELINES FOR ETHICS DOCUMENTS
https://www.wjgnet.com/bpg/GerInfo/287

GUIDELINES FOR NON-NATIVE SPEAKERS OF ENGLISH
https://www.wjgnet.com/bpg/gerinfo/240

PUBLICATION ETHICS
https://www.wjgnet.com/bpg/GerInfo/288

PUBLICATION MISCONDUCT
https://www.wjgnet.com/bpg/gerinfo/208

ARTICLE PROCESSING CHARGE
https://www.wjgnet.com/bpg/gerinfo/242

STEPS FOR SUBMITTING MANUSCRIPTS
https://www.wjgnet.com/bpg/GerInfo/239

ONLINE SUBMISSION
https://www.f6publishing.com

World Journal of Radiology

Submit a Manuscript: https://www.f6publishing.com

World J Radiol 2024 January 28; 16(1): 1-8

DOI: 10.4329/wjr.v16.i1.1

ISSN 1949-8470 (online)

MINIREVIEWS

Anti-N-methyl-D-aspartate receptor-associated encephalitis: A review of clinicopathologic hallmarks and multimodal imaging manifestations

Bryce David Beutler, Alastair E Moody, Jerry Mathew Thomas, Benjamin Phillip Sugar, Mark B Ulanja, Daniel Antwi-Amoabeng, Lucas Anthony Tsikitas

Specialty type: Radiology, nuclear medicine and medical imaging

Provenance and peer review: Invited article; Externally peer reviewed.

Peer-review model: Single blind

Peer-review report's scientific quality classification

Grade A (Excellent): A
Grade B (Very good): 0
Grade C (Good): 0
Grade D (Fair): D
Grade E (Poor): 0

P-Reviewer: Miao MS, China

Received: September 30, 2023
Peer-review started: September 30, 2023
First decision: November 30, 2023
Revised: December 4, 2023
Accepted: December 25, 2023
Article in press: December 25, 2023
Published online: January 28, 2024

Bryce David Beutler, Jerry Mathew Thomas, Benjamin Phillip Sugar, Lucas Anthony Tsikitas, Department of Radiology, University of Southern California, Keck School of Medicine, Los Angeles, CA 90033, United States

Alastair E Moody, Department of Anesthesiology, University of Utah, Salt Lake City, UT 84132, United States

Mark B Ulanja, Daniel Antwi-Amoabeng, Department of Internal Medicine, Christus Ochsner St. Patrick Hospital, Lake Charles, LA 70601, United States

Corresponding author: Bryce David Beutler, MD, Doctor, Department of Radiology, University of Southern California, Keck School of Medicine, 1500 San Pablo Street, 2nd Floor, Los Angeles, CA 90033, United States. brycebeutler@hotmail.com

Abstract

Anti-N-methyl-D-aspartate receptor-associated encephalitis (NMDARE) is a rare immune-mediated neuroinflammatory condition characterized by the rapid onset of neuropsychiatric symptoms and autonomic dysfunction. The mechanism of pathogenesis remains incompletely understood, but is thought to be related to antibodies targeting the GluN1 subunit of the NMDA receptor with resultant downstream dysregulation of dopaminergic pathways. Young adults are most frequently affected; the median age at diagnosis is 21 years. There is a strong female predilection with a female sex predominance of 4:1. NMDARE often develops as a paraneoplastic process and is most commonly associated with ovarian teratoma. However, NMDARE has also been described in patients with small cell lung cancer, clear cell renal carcinoma, and other benign and malignant neoplasms. Diagnosis is based on correlation of the clinical presentation, electroencephalography, laboratory studies, and imaging. Computed tomography, positron emission tomography, and magnetic resonance imaging are essential to identify an underlying tumor, exclude clinicopathologic mimics, and predict the likelihood of long-term functional impairment. Nuclear imaging may be of value for prognostication and to assess the response to therapy. Treatment may involve high-dose corticosteroids, intravenous immunoglobulin, and plasma exchange. Herein, we review the hallmark clinicopathologic features and imaging findings of this rare but potentially devastating condition and summarize diagnostic

criteria, treatment regimens, and proposed pathogenetic mechanisms.

Key Words: Anti-N-methyl-D-aspartate receptor-associated encephalitis; Autoimmune encephalitis; Encephalitis; Ovarian teratoma; Paraneoplastic syndrome; Teratoma

Core Tip: Anti-N-methyl-D-aspartate receptor-associated encephalitis (NMDARE) is a rare immune-mediated neuroinflammatory condition characterized by the rapid onset of neuropsychiatric symptoms and autonomic dysfunction. The key clinicopathologic and imaging features of NMDARE are detailed in this minireview, including validated diagnostic criteria, magnetic resonance imaging findings, differential considerations, pathogenetic mechanisms, and treatment regimens. In addition, the role of nuclear imaging – including positron emission tomography and single-photon emission computed tomography – is described with the salient findings detailed in a comprehensive table.

Citation: Beutler BD, Moody AE, Thomas JM, Sugar BP, Ulanja MB, Antwi-Amoabeng D, Tsikitas LA. Anti-N-methyl-D-aspartate receptor-associated encephalitis: A review of clinicopathologic hallmarks and multimodal imaging manifestations. *World J Radiol* 2024; 16(1): 1-8
URL: https://www.wjgnet.com/1949-8470/full/v16/i1/1.htm
DOI: https://dx.doi.org/10.4329/wjr.v16.i1.1

INTRODUCTION

Anti-N-methyl-D-aspartate receptor-associated encephalitis (NMDARE) is a rare immune-mediated neuroinflammatory condition characterized by the rapid onset of neuropsychiatric symptoms and autonomic dysfunction. NMDARE may be idiopathic, but often occurs as a paraneoplastic process in the setting of small cell lung carcinoma, ovarian teratoma, and other benign and malignant neoplasms[1,2]. A significant majority of patients diagnosed with NMDARE are young adults ranging in age from 18 years to 42 years[3]. The mechanism of pathogenesis remains incompletely understood[4].

The clinical presentation of NMDARE is variable and may include vague prodromal symptoms, such as headache and nausea, followed by the rapid development of cognitive dysfunction, behavioral changes, and central hypoventilation[5]. Careful correlation of clinical history, electroencephalography (EEG), and imaging is required to establish a presumptive diagnosis; serology or cerebrospinal fluid analysis is the gold standard for definitive diagnosis, with the presence of anti-GluN IgG antibodies constituting a positive result. Management may involve high-dose corticosteroids, intravenous immunoglobulin, and immunotherapy[6].

Herein, we review the clinicopathologic and imaging hallmarks of NMDARE and discuss management strategies for this rare but potentially devastating syndrome.

HISTORY OF NMDARE

The first cases of NMDARE were reported by Dalmau *et al*[7] in 2007, who described a small group of patients who presented with neuropsychiatric symptoms and were subsequently found to have antibodies to the NMDA receptor in blood or cerebrospinal fluid. One year later, Dalmau *et al*[7] launched a case-control study in which they detailed the clinical characteristics – including symptoms, management, and outcomes – of 100 patients with antibody-positive NMDARE[8]. The syndrome was subsequently thrust into the mainstream consciousness when a prominent New York Post journalist, Susannah Cahalan, was diagnosed with NMDARE; her experience as a patient is detailed in the bestselling memoir *Brain on Fire*[9]. The following years were defined by an explosion of NMDARE research, culminating in the establishment of validated diagnostic criteria and consensus practice guidelines.

DIAGNOSTIC CRITERIA

The hallmark clinical features, therapeutic regimens, and outcomes of paraneoplastic and non-paraneoplastic NMDARE were described in a multi-institutional observational study conducted by Titulaer *et al*[3] in 2013. Graus, Titulaer, and colleagues subsequently proposed three diagnostic criteria that could be used to establish a diagnosis of probable NMDARE: (1) Rapid onset of at least four of six classic symptoms; (2) an abnormal EEG or cerebrospinal fluid analysis showing pleocytosis or oligoclonal bands; and (3) reasonable exclusion of other disorders[5]. Graus and Titulaer proposed that a definitive diagnosis could be established with positive IgG anti-GluN1 antibodies in the presence of the aforementioned clinical criteria.

The diagnostic criteria introduced by Graus and Titulaer has served as a foundational guide for the assessment of suspected NMDARE. However, two key clinical features are not included in the criteria: (1) A history of benign or malignant neoplasm and (2) imaging features. NMDARE develops as a paraneoplastic process in up to 60% of cases[8]. Mature or immature ovarian teratomas are by far the most common underlying tumors and a known ovarian teratoma is included as a modifier within the Graus diagnostic criteria. However, NMDARE has also been described in the setting of small cell lung cancer, clear cell renal carcinoma, chronic myelogenous leukemia, pancreatic neuroendocrine tumor, and many other benign and malignant neoplasms[2,10]. The presence of a neoplasm or history of cancer therefore represents an important clinical finding that favors NMDARE over other encephalitides or neuropsychiatric disorders.

IMAGING FEATURES OF NMDARE

Imaging, including computed tomography (CT), positron emission tomography (PET), and magnetic resonance imaging (MRI), plays a central role in the evaluation of NMDARE. The utility of imaging is two-fold: (1) To identify an underlying primary neoplasm and (2) to exclude clinicopathologic mimics of NMDARE. Common causes of neuropsychiatric symptoms in young adults include herpes encephalitis, drug intoxication, and central nervous system vasculitides, all of which demonstrate imaging features that are distinct from those of NMDARE[11]. For example, herpes encephalitis is classically characterized by asymmetric T2/FLAIR hyperintensity within the medial temporal lobes whereas opioid intoxication may show symmetric T2/FLAIR hyperintensity within the posterior limb of the internal capsule. The imaging differential diagnosis for NMDARE is further detailed in Table 1.

The magnetic resonance imaging manifestations of NMDARE within the central nervous system are variable. Zhang *et al*[12] introduced a classification schema that can be used to evaluate T2/FLAIR hyperintense lesions in patients with NMDARE, which categorizes patients into four distinct categories based on distribution: Type 1 – normal brain MRI; type 2 – lesions within the hippocampus; type 3 – lesions involving structures other than the hippocampus; and type 4 – lesions within the hippocampus and other structures within the supratentorial or infratentorial brain parenchyma. A normal brain MRI, or a type 1 pattern, is present in approximately half of patients with a serologically confirmed diagnosis and typically portends a favorable outcome. The type 4 pattern is the second most common and has been associated with poor functional outcomes. The type 2 pattern is seen with intermediate frequency and is associated with relatively poor outcomes. Type 3 patterns are seen with intermediate frequency and are most often associated with positive outcomes, although some degree of long-term functional impairment may occur in some individuals.

Supratentorial and infratentorial T2/FLAIR hyperintense brain lesions with a slight hippocampal predilection represent the imaging hallmark of NMDARE. However, other central nervous system manifestations have been described, including myelitis, optic neuritis, and isolated meningitis[13,14]. The prodromal and neuropsychiatric symptoms are similar even in the setting of atypical lesions and the presence of spinal cord or cranial nerve lesions does not exclude an NMDARE diagnosis. Lesions in unusual locations can affect symptomatology, and patients may present with visual disturbances, hemiparesis, and other neurologic deficits superimposed upon the classic psychotic symptoms that typify NMDARE. Correlation of clinical history, laboratory studies, and comprehensive neuraxis imaging is therefore essential to establish a diagnosis.

Magnetic resonance spectroscopy (MRS) may also be of value for the assessment of suspected NMDARE. In a case report by Kataoka *et al*[15], authors described a reduced *N*-acetylasparate (NAA) peak with a decreased NAA/creatine ratio and a slightly increased choline peak within the basal ganglia, suggestive of diminished neuronal activity in the setting of neuroinflammation; the abnormal MRS findings improved following treatment of the underlying NMDARE. Splendiani *et al*[16] described similar findings in a subsequent report. The underlying cause of metabolic dysfunction and the prognostic value of abnormal MRS findings remain to be established.

NUCLEAR MEDICINE AND MOLECULAR IMAGING IN NMDARE

Nuclear imaging can play an important role in the evaluation and management of NMDARE[17]. Brain ^{18}F-fluorodeoxyglucose (FDG) PET has emerged as a valuable modality to distinguish NMDARE from other autoimmune encephalopathies. In a systematic review by Morbelli *et al*[18], authors described several distinct patterns of cerebral hyper- and hypometabolism correlating with different autoantibodies. NDMARE was characterized by normal or increased metabolic activity within the frontal lobes with marked parieto-occipital hypometabolism. Limbic encephalitis with anti-LGI-1 antibodies, in contrast, was associated with temporal hypermetabolism and fronto-occipital hypometabolism. A subsequent study by Jha *et al*[19] revealed other cerebral metabolic patterns unique to specific autoimmune encephalopathies, including frontal lobe and basal ganglia hypermetabolism in anti-CASPR2 encephalitis and basal ganglia hypermetabolism with concurrent temporal lobe hypometabolism in anti-GAD encephalitis (Table 2)[19,20]. The degree of cerebral hypo- or hypermetabolism may correlate with disease severity and outcomes, although further research is necessary to clarify the prognostic value of brain FDG PET in autoimmune encephalopathies[21,22].

Other nuclear imaging studies that may be of value for the assessment of suspected NMDARE include whole-body FDG PET/CT scan, which is highly sensitive for the detection of occult malignancies, including ovarian teratoma and other neoplasms that have been associated with NMDARE[17]. Single photon emission computed tomography (SPECT) with technetium-99 hexamethyl propylenamine oxamine (HMPAO) and N-isopropyl-p-123-I-iodoampheatmine (I-123-IMP) have also been used to help diagnose NMDARE and may help identify cerebral metabolic abnormalities in the setting of a normal brain MRI and FDG PET[23,24]. The multimodal imaging features of NMDARE are further detailed in

Table 1 Magnetic resonance imaging differential diagnosis for anti-N-methyl-D-aspartate receptor-associated encephalitis

Condition	Classic imaging manifestations
NMDARE	T2/FLAIR hyperintense lesions that frequently involve the hippocampus or bilateral hippocampi
	Lesions within the infratentorial brain parenchyma and spinal cord are uncommon
	Leptomeningeal enhancement is occasionally present
Acute disseminated encephalomyelitis	Areas of high T2/FLAIR signal, predominantly within the subcortical white matter
	An "open ring" pattern of enhancement, similar to multiple sclerosis
	Lesions with peripheral diffusion restriction
Central nervous system vasculitis/PACNS	Foci of T2/FLAIR hyperintensity within the periventricular white matter or along watershed zones
	Parenchymal microhemorrhages may be present on GRE/SWI sequences
	Evidence of acute, subacute, or chronic stroke within a discrete vascular territory is present in some individuals
Creutzfeldt-Jakob disease	Symmetric T2/FLAIR hyperintensity involving the pulvinar and dorsomedial thalamic nuclei
	Diffusion restriction with concomitant T2 shine through is often present
Heroin inhalational leukoencephalopathy	Symmetric T2/FLAIR hyperintensity within the posterior limb of the internal capsules, which may extend inferiorly to the pontine corticospinal tracts
	Symmetric T2/FLAIR hyperintensity within the cerebellar white matter with sparing of the dentate nuclei
Herpes simplex encephalitis	Asymmetric T1 hypointense/T2 hyperintense edema involving the bilateral medial temporal lobes and insular cortex
	Gyral or leptomeningeal enhancement may be present
	Diffusion restriction is sometimes present
	Blooming on GRE/SWI sequences may be present in the setting of hemorrhage
Methanol poisoning	Symmetric or asymmetric T1 hyperintensity within the putamina, indicative of necrosis
	Asymmetric blooming within the putamina on GRE/SWI sequences in the setting of hemorrhage
Multiple sclerosis	Periventricular, cortical, or juxtacortical T2/FLAIR hyperintense lesions disseminated in space and time
	Infratentorial and spinal cord T2/FLAIR hyperintense lesions may develop in some individuals
	An "open ring" pattern of enhancement is present in active disease
Neuromyelitis optica	Optic nerve edema with T2/FLAIR hyperintense signal and, in some patients, optic nerve enhancement
	High T2/FLAIR signal within the spinal cord spanning at least three contiguous vertebral segments
	Brain parenchymal lesions are often absent

GRE: Gradient echo; NMDARE: Anti-N-methyl-D-aspartate receptor-associated encephalitis; PACNS: Primary angiitis of the central nervous system; SWI: Susceptibility weighted imaging.

Table 3.

MECHANISM OF PATHOGENESIS

The mechanism of pathogenesis for NMDARE remains to be established. Antibodies targeting the GluN1 subunit of the NMDA receptor are present in both paraneoplastic and non-paraneoplastic NMDARE; a juxtaposed T-cell mediated response is thought to occur only in paraneoplastic NMDARE[25]. The neuropsychiatric symptoms of NMDARE may be related to antibody-mediated blockade of NMDA receptors in the presynaptic gamma-aminobutyric acid ergic neurons of the thalamus and frontal cortex with resultant downstream dysregulation of dopaminergic pathways[26]. Indeed, the clinical hallmarks of NMDARE, including confusion, paranoia, and delusions, mirror those of psychosis; thus, hyperactive dopaminergic signal transduction may represent a shared mechanism underlying both conditions. Seizures are also common in NMDARE and may be related to excessive extrasynaptic NMDA receptor signaling. In a recent EEG study by Symmonds *et al*[27], authors observed aberrant NMDA signaling predominantly affecting NMDA receptors of excitatory neurons. However, despite the increasingly robust clinical data, the complex interplay between anti-NMDA antibodies, NMDA receptors, and dopaminergic pathways remains incompletely understood. Further research is necessary to establish a unifying model to account for the unique constellation of neuropsychiatric and autonomic symptoms that characterize NMDARE.

Table 2 Cerebral metabolic patterns of autoimmune encephalopathies[18-20]

Autoantibody	Metabolic pattern
Anti-NMDA receptor	Bifrontal hypermetabolism or normal frontal lobe metabolism
	Marked bilateral parieto-occipital hypometabolism
Anti-LGI-1	Bitemporal hypermetabolism
	Bilateral fronto-occipital hypometabolism
Anti-CASPR2	Bifrontal hypermetabolism
	Basal ganglia hypermetabolism
	Bilateral temporo-parietal hypometabolism
Anti-GAD-65	Bilateral basal ganglia hypometabolism
	Bitemporal hypometabolism
Anti-Hu	Bitemporal hypermetabolism

CASPR2: Anti-contactin-associated protein 2; GAD-65: Anti-glutamic acid decarboxylase; LGI-1: Leucine-rich glioma inactivated; NMDA: Anti-N-methyl-D-aspartate receptor.

Table 3 Multimodal imaging of anti-N-methyl-D-aspartate receptor-associated encephalitis[12-24]

Ultrasound	Pelvic or scrotal ultrasound may be used to identify an underlying teratoma in the appropriate patient population
	Ultrasound-guided lymph node biopsy may be required in the setting of metastatic disease with no known primary
MRI	A normal brain MRI is present in half of patients with NMDARE
	T2/FLAIR hyperintense lesions are most commonly present within the supratentorial brain parenchyma and may correlate with prognosis:
	Type 1: Normal brain MRI; favorable prognosis
	Type 2: Hippocampal lesions only; poor prognosis
	Type 3: Lesions involving structures other than the hippocampus; intermediate prognosis
	Type 4: Lesions involving both the hippocampus and other brain structures; poor prognosis
	Infratentorial, spinal cord, and cranial nerve lesions are less common, but may occur in some individuals
	Leptomeningeal enhancement is rare, but has been described
MRS	Reduced NAA peak
	Decreased NAA/creatine ratio
	Increased choline peak
FDG PET	Brain FDG PET classically shows bifrontal hypermetabolism with parieto-occipital hypometabolism
	The frontal-to-parietooccipital metabolic gradient may correlate with prognosis, with an increased gradient portending a worse outcome
	Whole-body FDG PET may be of value to identify a primary neoplasm and/or localize a lesion for image-guided biopsy
SPECT	HMPAO and I-123-IMP SPECT may be useful for metabolic evaluation in patients with clinical features of NMDARE and a normal brain MRI and FDG PET

FDG PET: Fludeoxyglucose positron emission tomography; HMPAO: Technetium-99 hexamethyl propylenamine oxamine; I-123-IMP: N-isopropyl-p-123-I-iodoamphetamine; MRI: Magnetic resonance imaging; MRS: Magnetic resonance spectroscopy; NAA: N-acetylaspartate; NMDARE: Anti-N-methyl-D-aspartate receptor-associated encephalitis; SPECT: Single-photon emission computed tomography.

MANAGEMENT OF NMDARE

There are no established clinical practice guidelines for the management of NMDARE. Supportive care is essential for most patients and may include benzodiazepines, anti-epileptic drugs, beta-blockers, anticholinergics, and close monitoring in the intensive care unit[28]. High-dose corticosteroids, intravenous immunoglobulin, and/or plasma exchange represent the mainstay of management for the underlying autoimmune dysfunction[29]. Immunotherapy, such as rituximab and cyclophosphamide, may serve as effective second-line agents. Agitation, hallucinations, and delusions may be challenging to manage in NMDARE patients and benzodiazepines often do not provide adequate sedation; ketamine or propofol may be required for some individuals. Catatonia may occur in some patients and may improve with high-dose benzodiazepines or electroconvulsive therapy[30]. Pregnant patients represent a special population occasionally affected by NMDARE. The limited existing data suggest that high-dose corticosteroids are safe and effective, but second-line agents – including rituximab and cyclophosphamide – should be avoided in pregnancy due to the risk of teratogenicity.

Clinical monitoring and follow-up of NMDARE is distinct from that of many other encephalitides. Acute disseminated encephalomyelitis, herpes encephalitis, and other similar neuroinflammatory conditions typically resolve or improve within days of treatment initiation. However, clinical resolution of NMDARE may require many weeks or months; functional improvements have been observed over 2 years after resolution of the acute phase of illness[3]. The current consensus guidelines suggest that treatment with a first- or second-line agent should be continued for at least 6 wk before clinical re-evaluation and escalation or discontinuation of therapy[31]. Dose escalation or transition from a first- to second-line agent may be considered before 6 wk in the setting of severe illness with autonomic dysfunction. Physical and occupational therapy – including mobility training, gait training, and speech-language therapy – play a key role in improving long-term functional outcomes and is recommended for nearly all patients with an NMDARE diagnosis[32].

CONCLUSION

NMDARE represents a rare immune-mediated clinical entity that presents with a unique constellation of neuropsychiatric and autonomic symptoms. Early diagnosis and management is essential to prevent catastrophic outcomes or death. A presumptive diagnosis can be established through careful correlation of clinical history, EEG, and imaging studies. However, cerebrospinal fluid analysis is the gold standard diagnostic test, with the presence of IgG anti-GluN1 antibodies allowing for definitive diagnosis.

High-dose corticosteroids, intravenous immunoglobulin, and plasma exchange are first-line therapies for NMDARE. Rituximab or cyclophosphamide may be required for some individuals. Nearly all patients with NMDARE will require supportive care, which may include sedatives, airway protection, and close monitoring in the intensive care unit. The prognosis for patients with NMDARE is variable; the existing data suggest that patients presenting without hippocampal lesions on MRI tend to experience relatively favorable outcomes. Nuclear imaging may also be of value for prognostication, as emerging evidence indicates that cerebral metabolic gradients on FDG PET may help predict functional outcomes.

The underlying mechanism of pathogenesis for NMDARE remains to be established, although most authors agree that dopaminergic pathways are implicated in the neuropsychiatric symptoms. Neuroinflammation may also play an important role in the pathogenesis of NMDARE but cannot yet be diagnosed by imaging or by routine laboratory studies.

Imaging will undoubtedly play a central role in NMDARE diagnosis in the future. Widespread adoption of the MRI classification schema introduced by Zhang *et al*[12] may improve diagnostic accuracy and provide important prognostic information to help guide clinical management. In addition, brain FDG PET can currently be used to identify patterns of cerebral metabolism suggestive of underlying NMDARE. However, advancements in molecular imaging and the development of novel radiotracers may allow for detection of aberrant proteins that are expressed early in the disease process. It has been definitively established that early intervention portends better patient outcomes; multimodal imaging will be vital to ensure timely and accurate diagnosis and expedited management. Future research is needed to develop targeted therapies and improve clinical outcomes for patients who develop this rare but potentially devastating immune-mediated condition.

FOOTNOTES

Author contributions: Beutler BD performed the majority of the writing; Moody AE prepared the tables; Thomas JM and Sugar BP assisted with the literature review; Ulanja MB and Antwi-Amoabeng D contributed to the sections on pathogenesis and management; Tsikitas LA designed the outline and coordinated the writing of the paper.

Conflict-of-interest statement: None of the authors have real or potential conflicts of interest.

Country/Territory of origin: United States

ORCID number: Bryce David Beutler 0000-0002-5071-1826; Alastair E Moody 0000-0002-5232-7705; Mark B Ulanja 0000-0001-5966-3966; Daniel Antwi-Amoabeng 0000-0001-8594-004X.

S-Editor: Liu JH
L-Editor: Filipodia
P-Editor: Zhao S

REFERENCES

1 **Bost C**, Chanson E, Picard G, Meyronet D, Mayeur ME, Ducray F, Rogemond V, Psimaras D, Antoine JC, Delattre JY, Desestret V, Honnorat J. Malignant tumors in autoimmune encephalitis with anti-NMDA receptor antibodies. *J Neurol* 2018; **265**: 2190-2200 [PMID: 30003358 DOI: 10.1007/s00415-018-8970-0]
2 **Yang J**, Li B, Li X, Lai Z. Anti-N-Methyl-D-Aspartate Receptor Encephalitis Associated With Clear Cell Renal Carcinoma: A Case Report. *Front Oncol* 2020; **10**: 350 [PMID: 32292718 DOI: 10.3389/fonc.2020.00350]
3 **Titulaer MJ**, McCracken L, Gabilondo I, Armangué T, Glaser C, Iizuka T, Honig LS, Benseler SM, Kawachi I, Martinez-Hernandez E, Aguilar E, Gresa-Arribas N, Ryan-Florance N, Torrents A, Saiz A, Rosenfeld MR, Balice-Gordon R, Graus F, Dalmau J. Treatment and prognostic factors for long-term outcome in patients with anti-NMDA receptor encephalitis: an observational cohort study. *Lancet Neurol* 2013; **12**: 157-165 [PMID: 23290630 DOI: 10.1016/S1474-4422(12)70310-1]
4 **Lynch DR**, Rattelle A, Dong YN, Roslin K, Gleichman AJ, Panzer JA. Anti-NMDA Receptor Encephalitis: Clinical Features and Basic Mechanisms. *Adv Pharmacol* 2018; **82**: 235-260 [PMID: 29413523 DOI: 10.1016/bs.apha.2017.08.005]
5 **Graus F**, Titulaer MJ, Balu R, Benseler S, Bien CG, Cellucci T, Cortese I, Dale RC, Gelfand JM, Geschwind M, Glaser CA, Honnorat J, Höftberger R, Iizuka T, Irani SR, Lancaster E, Leypoldt F, Prüss H, Rae-Grant A, Reindl M, Rosenfeld MR, Rostásy K, Saiz A, Venkatesan A, Vincent A, Wandinger KP, Waters P, Dalmau J. A clinical approach to diagnosis of autoimmune encephalitis. *Lancet Neurol* 2016; **15**: 391-404 [PMID: 26906964 DOI: 10.1016/S1474-4422(15)00401-9]
6 **Kadoya M**, Onoue H, Kadoya A, Ikewaki K, Kaida K. Refractory status epilepticus caused by anti-NMDA receptor encephalitis that markedly improved following combination therapy with rituximab and cyclophosphamide. *Intern Med* 2015; **54**: 209-213 [PMID: 25743014 DOI: 10.2169/internalmedicine.54.2047]
7 **Dalmau J**, Bataller L. [Limbic encephalitis: the new cell membrane antigens and a proposal of clinical-immunological classification with therapeutic implications]. *Neurologia* 2007; **22**: 526-537 [PMID: 18000762]
8 **Dalmau J**, Gleichman AJ, Hughes EG, Rossi JE, Peng X, Lai M, Dessain SK, Rosenfeld MR, Balice-Gordon R, Lynch DR. Anti-NMDA-receptor encephalitis: case series and analysis of the effects of antibodies. *Lancet Neurol* 2008; **7**: 1091-1098 [PMID: 18851928 DOI: 10.1016/S1474-4422(08)70224-2]
9 **Susannah C**. Brain on Fire: My Month of Madness. Free Press, 2012
10 **Yu Y**, Liu JL, Tian DS. Anti-N-methyl-D-aspartate receptor encephalitis associated with chronic myelogenous leukemia, causality or coincidence? A case report. *BMC Neurol* 2022; **22**: 153 [PMID: 35461209 DOI: 10.1186/s12883-022-02675-5]
11 **Yu Y**, Wu Y, Cao X, Li J, Liao X, Wei J, Huang W. The Clinical Features and Prognosis of Anti-NMDAR Encephalitis Depends on Blood Brain Barrier Integrity. *Mult Scler Relat Disord* 2021; **47**: 102604 [PMID: 33130468 DOI: 10.1016/j.msard.2020.102604]
12 **Zhang T**, Duan Y, Ye J, Xu W, Shu N, Wang C, Li K, Liu Y. Brain MRI Characteristics of Patients with Anti-N-Methyl-D-Aspartate Receptor Encephalitis and Their Associations with 2-Year Clinical Outcome. *AJNR Am J Neuroradiol* 2018; **39**: 824-829 [PMID: 29567651 DOI: 10.3174/ajnr.A5593]
13 **Outteryck O**, Baille G, Hodel J, Giroux M, Lacour A, Honnorat J, Zéphir H, Vermersch P. Extensive myelitis associated with anti-NMDA receptor antibodies. *BMC Neurol* 2013; **13**: 211 [PMID: 24373538 DOI: 10.1186/1471-2377-13-211]
14 **Mugavin M**, Mueller BH 2nd, Desai M, Golnik KC. Optic Neuropathy As the Initial Presenting Sign of N-methyl-d-aspartate (NMDA) Encephalitis. *Neuroophthalmology* 2017; **41**: 90-93 [PMID: 28348631 DOI: 10.1080/01658107.2016.1262431]
15 **Kataoka H**, Dalmau J, Taoka T, Ueno S. Reduced N-acetylaspartate in the basal ganglia of a patient with anti-NMDA receptor encephalitis. *Mov Disord* 2009; **24**: 784-786 [PMID: 19217070 DOI: 10.1002/mds.22167]
16 **Splendiani A**, Felli V, Di Sibio A, Gennarelli A, Patriarca L, Stratta P, Di Cesare E, Rossi A, Massimo G. Magnetic resonance imaging and magnetic resonance spectroscopy in a young male patient with anti-N-methyl-D-aspartate receptor encephalitis and uncommon cerebellar involvement: A case report with review of the literature. *Neuroradiol J* 2016; **29**: 30-35 [PMID: 26613928 DOI: 10.1177/1971400915609333]
17 **Wang M**, Jiang S, Zhang Y, Jiang C, Xia F, Lyu W, Ma X. The application of 18F-FDG PET/CT in ovarian immature teratomas when pathological examination results contradict clinical observations: a case report. *Medicine (Baltimore)* 2017; **96**: e9171 [PMID: 29390326 DOI: 10.1097/MD.0000000000009171]
18 **Morbelli S**, Zoccarato M, Bauckneht M, Anglani M, Cecchin D. 18F-FDG-PET and MRI in autoimmune encephalitis: a systematic review of brain findings. *Clin Transl Imaging* 2018; **6**: 151-168 [DOI: 10.1007/s40336-018-0275-x]
19 **Jha S**, Nagaraj C, Mundlamuri RC, Alladi S, Nashi S, Kenchaiah R, Mahadevan A, Bhat M, Saini J, Netravathi M. FDG-PET in Autoimmune Encephalitis: Utility, Pattern of Abnormalities, and Correlation with Autoantibodies. *Ann Indian Acad Neurol* 2022; **25**: 1122-1129 [PMID: 36911487 DOI: 10.4103/aian.aian_645_22]
20 **Bordonne M**, Chawki MB, Doyen M, Kas A, Guedj E, Tyvaert L, Verger A. Brain (18)F-FDG PET for the diagnosis of autoimmune encephalitis: a systematic review and a meta-analysis. *Eur J Nucl Med Mol Imaging* 2021; **48**: 3847-3858 [PMID: 33677643 DOI: 10.1007/s00259-021-05299-y]
21 **Leypoldt F**, Buchert R, Kleiter I, Marienhagen J, Gelderblom M, Magnus T, Dalmau J, Gerloff C, Lewerenz J. Fluorodeoxyglucose positron emission tomography in anti-N-methyl-D-aspartate receptor encephalitis: distinct pattern of disease. *J Neurol Neurosurg Psychiatry* 2012; **83**: 681-686 [PMID: 22566598 DOI: 10.1136/jnnp-2011-301969]
22 **Maeder-Ingvar M**, Prior JO, Irani SR, Rey V, Vincent A, Rossetti AO. FDG-PET hyperactivity in basal ganglia correlating with clinical

course in anti-NDMA-R antibodies encephalitis. *J Neurol Neurosurg Psychiatry* 2011; **82**: 235-236 [PMID: 20667855 DOI: 10.1136/jnnp.2009.198697]

23 **Llorens V**, Gabilondo I, Gómez-Esteban JC, Agundez M, Mendibe M, Bergara JC, Ciordia R, Saiz A, Zarranz JJ. Abnormal multifocal cerebral blood flow on Tc-99m HMPAO SPECT in a patient with anti-NMDA-receptor encephalitis. *J Neurol* 2010; **257**: 1568-1569 [PMID: 20352245 DOI: 10.1007/s00415-010-5546-z]

24 **Higashiyama A**, Komori T, Osuga K. 123I-IMP SPECT findings in anti-NMDA receptor encephalitis. *J Nucl Med* 2020; **61**: 1575

25 **Dalmau J**, Graus F. Antibody-Mediated Encephalitis. *N Engl J Med* 2018; **378**: 840-851 [PMID: 29490181 DOI: 10.1056/NEJMra1708712]

26 **Barry H**, Byrne S, Barrett E, Murphy KC, Cotter DR. Anti-N-methyl-d-aspartate receptor encephalitis: review of clinical presentation, diagnosis and treatment. *BJPsych Bull* 2015; **39**: 19-23 [PMID: 26191419 DOI: 10.1192/pb.bp.113.045518]

27 **Symmonds M**, Moran CH, Leite MI, Buckley C, Irani SR, Stephan KE, Friston KJ, Moran RJ. Ion channels in EEG: isolating channel dysfunction in NMDA receptor antibody encephalitis. *Brain* 2018; **141**: 1691-1702 [PMID: 29718139 DOI: 10.1093/brain/awy107]

28 **Abboud H**, Probasco J, Irani SR, Ances B, Benavides DR, Bradshaw M, Christo PP, Dale RC, Fernandez-Fournier M, Flanagan EP, Gadoth A, George P, Grebenciucova E, Jammoul A, Lee ST, Li Y, Matiello M, Morse AM, Rae-Grant A, Rojas G, Rossman I, Schmitt S, Venkatesan A, Vernino S, Pittock SJ, Titulaer M; Autoimmune Encephalitis Alliance Clinicians Network. Autoimmune encephalitis: proposed recommendations for symptomatic and long-term management. *J Neurol Neurosurg Psychiatry* 2021; **92**: 897-907 [PMID: 33649021 DOI: 10.1136/jnnp-2020-325302]

29 **Huang Q**, Xie Y, Hu Z, Tang X. Anti-N-methyl-D-aspartate receptor encephalitis: A review of pathogenic mechanisms, treatment, prognosis. *Brain Res* 2020; **1727**: 146549 [PMID: 31726044 DOI: 10.1016/j.brainres.2019.146549]

30 **Wu H**, Wu C, Zhou Y, Huang S, Zhu S. Catatonia in adult anti-NMDAR encephalitis: an observational cohort study. *BMC Psychiatry* 2023; **23**: 94 [PMID: 36750806 DOI: 10.1186/s12888-022-04505-x]

31 **Nosadini M**, Thomas T, Eyre M, Anlar B, Armangue T, Benseler SM, Cellucci T, Deiva K, Gallentine W, Gombolay G, Gorman MP, Hacohen Y, Jiang Y, Lim BC, Muscal E, Ndondo A, Neuteboom R, Rostásy K, Sakuma H, Sharma S, Tenembaum SN, Van Mater HA, Wells E, Wickstrom R, Yeshokumar AK, Irani SR, Dalmau J, Lim M, Dale RC. International Consensus Recommendations for the Treatment of Pediatric NMDAR Antibody Encephalitis. *Neurol Neuroimmunol Neuroinflamm* 2021; **8** [PMID: 34301820 DOI: 10.1212/NXI.0000000000001052]

32 **Kennedy C**, O'Shea R, De Ranieri D. Physical Therapy Interventions and Outcome Measures for a Patient Diagnosed with Anti-NMDA Receptor Encephalitis. *Pediatr Ann* 2021; **50**: e437-e443 [PMID: 34617842 DOI: 10.3928/19382359-20210917-01]

World Journal of Radiology

Submit a Manuscript: https://www.f6publishing.com

World J Radiol 2024 January 28; 16(1): 9-19

DOI: 10.4329/wjr.v16.i1.9

ISSN 1949-8470 (online)

ORIGINAL ARTICLE

Retrospective Cohort Study

Computed tomography-based nomogram of Siewert type II/III adenocarcinoma of esophagogastric junction to predict response to docetaxel, oxaliplatin and S-1

Chuan-Qinyuan Zhou, Dan Gao, Yan Gui, Ning-Pu Li, Wen-Wen Guo, Hai-Ying Zhou, Rui Li, Jing Chen, Xiao-Ming Zhang, Tian-Wu Chen

Specialty type: Oncology

Provenance and peer review: Invited article; Externally peer reviewed.

Peer-review model: Single blind

Peer-review report's scientific quality classification

Grade A (Excellent): 0
Grade B (Very good): 0
Grade C (Good): 0
Grade D (Fair): D
Grade E (Poor): 0

P-Reviewer: Cerwenka H, Austria

Received: October 4, 2023
Peer-review started: October 4, 2023
First decision: November 30, 2023
Revised: December 13, 2023
Accepted: January 8, 2024
Article in press: January 8, 2024
Published online: January 28, 2024

Chuan-Qinyuan Zhou, Dan Gao, Wen-Wen Guo, Hai-Ying Zhou, Rui Li, Xiao-Ming Zhang, Department of Radiology, Affiliated Hospital of North Sichuan Medical College, Nanchong 637000, Sichuan Province, China

Yan Gui, Ning-Pu Li, Department of Oncology, Affiliated Hospital of North Sichuan Medical College, Nanchong 637000, Sichuan Province, China

Jing Chen, Department of Radiology, Sichuan Provincial People's Hospital, University of Electronic Science and Technology of China, Chengdu 610072, Sichuan Province, China

Tian-Wu Chen, Department of Radiology, The Second Affiliated Hospital of Chongqing Medical University, Chongqing 400010, China

Corresponding author: Tian-Wu Chen, MD, Dean, Director, Doctor, Full Professor, Department of Radiology, The Second Affiliated Hospital of Chongqing Medical University, No. 74 Linjiang Road, Yuzhong District, Chongqing 400010, China. tianwuchen_nsmc@163.com

Abstract

BACKGROUND

Neoadjuvant chemotherapy (NAC) has become the standard care for advanced adenocarcinoma of esophagogastric junction (AEG), although a part of the patients cannot benefit from NAC. There are no models based on baseline computed tomography (CT) to predict response of Siewert type II or III AEG to NAC with docetaxel, oxaliplatin and S-1 (DOS).

AIM

To develop a CT-based nomogram to predict response of Siewert type II/III AEG to NAC with DOS.

METHODS

One hundred and twenty-eight consecutive patients with confirmed Siewert type II/III AEG underwent CT before and after three cycles of NAC with DOS, and were randomly and consecutively assigned to the training cohort (TC) (n = 94) and the validation cohort (VC) (n = 34). Therapeutic effect was assessed by disease-control rate and progressive disease according to the Response Evaluation

Criteria in Solid Tumors (version 1.1) criteria. Possible prognostic factors associated with responses after DOS treatment including Siewert classification, gross tumor volume (GTV), and cT and cN stages were evaluated using pretherapeutic CT data in addition to sex and age. Univariate and multivariate analyses of CT and clinical features in the TC were performed to determine independent factors associated with response to DOS. A nomogram was established based on independent factors to predict the response. The predictive performance of the nomogram was evaluated by Concordance index (C-index), calibration and receiver operating characteristics curve in the TC and VC.

RESULTS

Univariate analysis showed that Siewert type (52/55 *vs* 29/39, $P = 0.005$), pretherapeutic cT stage (57/62 *vs* 24/32, $P = 0.028$), GTV (47.3 ± 27.4 *vs* 73.2 ± 54.3, $P = 0.040$) were significantly associated with response to DOS in the TC. Multivariate analysis of the TC also showed that the pretherapeutic cT stage, GTV and Siewert type were independent predictive factors related to response to DOS (odds ratio = 4.631, 1.027 and 7.639, respectively; all $P < 0.05$). The nomogram developed with these independent factors showed an excellent performance to predict response to DOS in the TC and VC (C-index: 0.838 and 0.824), with area under the receiver operating characteristic curve of 0.838 and 0.824, respectively. The calibration curves showed that the practical and predicted response to DOS effectively coincided.

CONCLUSION

A novel nomogram developed with pretherapeutic cT stage, GTV and Siewert type predicted the response of Siewert type II/III AEG to NAC with DOS.

Key Words: Esophagogastric junction; Adenocarcinoma; Neoadjuvant chemotherapy; Response; Tomography, X-ray computed; Predictor

Core Tip: We developed a computed-tomography-based nomogram with independent predictors including cT stage, gross tumor volume and Siewert type to predict the response of Siewert type II/III adenocarcinoma of the esophagogastric junction to neoadjuvant chemotherapy (NAC) with docetaxel, oxaliplatin and S-1 (DOS). The nomogram could predict subgroups of patients who would optimally benefit from NAC with DOS. Siewert type could be a novel predictor for response to NAC compared, which lays a foundation for follow-up studies.

Citation: Zhou CQ, Gao D, Gui Y, Li NP, Guo WW, Zhou HY, Li R, Chen J, Zhang XM, Chen TW. Computed tomography-based nomogram of Siewert type II/III adenocarcinoma of esophagogastric junction to predict response to docetaxel, oxaliplatin and S-1. *World J Radiol* 2024; 16(1): 9-19
URL: https://www.wjgnet.com/1949-8470/full/v16/i1/9.htm
DOI: https://dx.doi.org/10.4329/wjr.v16.i1.9

INTRODUCTION

The incidence of adenocarcinoma of esophagogastric junction (AEG) has increased worldwide, and the survival rate is unsatisfactory[1,2]. Currently, surgical resection is the primary treatment for AEG, but it is only suitable for early-stage patients[3]. Generally, most patients are diagnosed in the advanced stage, indicating that they are unsuitable for surgical resection. Multimodal treatment has become the standard of care for locally advanced AEG. Preoperative neoadjuvant chemotherapy (NAC) is designed to shrink the tumor to achieve a higher rate of complete resection[4]. Although there is no uniform NAC regimen for AEG patients, and the regimens differ regionally, some research has indicated superiority of a docetaxel-based regimen over the established regimens, including S-1 and oxaliplatin, and cisplatin and fluorouracil [5-8]. The Eastern Asia countries mostly used docetaxel, oxaliplatin and S-1 (DOS) as first-line NAC[7]. However, research has demonstrated that patients who do not respond to DOS have a significantly worse prognosis. For docetaxel-based regimens, the key is to select AEG patients who optimally benefit from DOS and who do not respond to DOS in clinical practice.

The optimal treatment choice for AEG relies on the TNM staging and anatomical location. To evaluate the TNM stage and location, endoscopic ultrasound and computed tomography (CT) are the most common choices at present. However, endoscopic ultrasound is an invasive examination and may cause mucosal injury and uncomfortable response. In addition, it is hard to perform endoscopic ultrasound if the tumor causes significant stenosis. Compared with endoscopic ultrasound, CT can clearly show the morphological characteristics of the tumor, in addition to cT stage, cN stage and location of the lesion, and can measure tumor diameter and volume to assess the response to NAC[9,10]. Beer *et al*[11] reported the early response of AEG after NAC could be predicted through gross tumor volume (GTV) on CT. Hofheinz *et*

al[12] compared the response of advanced gastric cancer after different treatments through the changes in diameter, and cT and cN stages on CT. To our knowledge, there is no report on the development of a model based on CT characteristics to predict the response to DOS for advanced AEG patients. Our study aimed to establish and validate a novel nomogram based on CT characteristics to predict response to DOS, which could be helpful to choose optimal treatment and avoid the toxicity of DOS.

MATERIALS AND METHODS

Patients

This study was conducted in accordance with the Declaration of Helsinki, and approved by the Ethics Committee of our hospital. Written informed consent was obtained from each participant before the study.

From October 2017 to January 2021, we collected 150 consecutive patients with biopsy-confirmed AEG. The T and N stages were clinically determined according to American Joint Committee on Cancer (eighth edition). AEG was classified as stage T_0 if there was no evidence of primary tumor, and T_1, T_2, T_3, and T_4 if tumors invaded the lamina propria or submucosa, invaded the muscularis propria or subserosa, penetrated the serosa (visceral peritoneum) without invasion of adjacent structures, and invaded adjacent structures, respectively. AEG was classified as stage N_0 if there were no metastatic lymph nodes, and N_1, N_2, and N_3 if there were one to two, three to six, and seven or more metastatic lymph nodes, respectively.

Patients were enrolled according to the following inclusion criteria: (1) Patients were diagnosed with AEG through gastroscopic biopsy and with locally advanced AEG confirmed by pretherapeutic CT (depth of tumor invasion > cT_2N+M_0), and met the National Comprehensive Cancer Network (NCCN) guidelines[13]; and (2) patients received DOS chemotherapy, and underwent thoracoabdominal contrast-enhanced CT (CECT) in our hospital after three cycles of NAC. The exclusion criteria were as follows: (1) The quality of CT images was poor (n = 2); (2) The clinical data were incomplete (n = 3); (3) Patients had contemporary or previous malignancies (n = 7); or (4) AEG was classified as Siewert type I according to the NCCN guidelines, and was treated as esophageal carcinoma (n = 4). We enrolled 134 patients. However, the number of cT_2 stage patients was too small (n = 6), and surgical treatment was mainly used in clinical practice. Therefore, we did not enroll cT_2 stage patients, and collected cT_{3-4} stage patients. As a result, we enrolled 128 consecutive cT_{3-4} stage patients who received DOS. All patients were randomly assigned to the training cohort (TC) and validation cohort (VC) at a ratio of 7:3, and the assignment was proportionally stratified by tumor location, cT stage, and cN stage. To ensure no distant metastases, positron emission tomography-CT was used before NAC. The clinical characteristics of the 128 enrolled patients are listed in Table 1.

The DOS treatment during each 3-week cycle was as follows. Docetaxel 75 mg/m^2 and oxaliplatin 130 mg/m^2 were administered by intravenous infusion on day 1. Based on the patient's body surface, S-1 was administered orally on days 1–14 (80, 100 and 120 mg/time in the case of body surface area < 1.25 m^2, 1.25–1.5 m^2 and ≥ 1.5 m^2, respectively).

CT image acquisition

All patients in our study underwent CT scans with two 64 multi-detector systems (LightSpeed VCT; GE Medical Systems, Milwaukee, WI, United States) 1 wk before initiation of NAC and after three cycles. Before each CT examination, all patients drank 500–1000 mL water as an oral negative contrast material. Patients were scanned in the supine position and held their breath for 10–15 s to obtain good quality images. After conventional CT without enhancement, biphasic enhancement CT scans were obtained 25 and 70 s after intravenous injection of 1.5 mL/kg contrast material (Omnipaque, Iohexol; GE Healthcare, Chicago, IL, United States) at a rate of 3.0 mL/s with a pump injector (Medrad; Vistron CT Injection System, Minneapolis MN, United States). The first-phase enhancement resulted in arterial phase images, and the second-phase enhancement resulted in portal venous phase images. The coverage of CT examination in the arterial phase was from the apex of the lungs to the middle of the right kidney to obtain thoracic enhanced images and abdominal arterial phase images. The coverage of CT in the portal venous phase was from the right diaphragmatic dome to the middle of the right kidney to obtain abdominal portal venous phase images. The CT scanning parameters were as follows: tube voltage 120 kV, tube current 200 mA, rotation time 0.5 s, detector collimation 64 mm × 0.6 mm, pitch 0.9, slice thickness 5 mm, slice interval 5 mm, and matrix 512 mm × 512 mm. The window settings were set with a width of 400 HU and window level of 40 HU.

Image-based treatment response evaluation

The treatment response in all target lesions including AEG and the positive lymph nodes was evaluated on CT according to the Response Evaluation Criteria in Solid Tumors, version 1.1 (RECIST 1.1) criteria[14]. Because the peak enhancement of AEG and abdominal lymph nodes was significantly higher in the portal venous phase compared with arterial phase, the response evaluation was analyzed through the abdominal portal venous phase images together with thoracic arterial phase enhanced images[15]. The treatment response of all target lesions after NAC was determined as follows: sum of maximal diameters (MDs) of AEG and positive nodal lesions before treatment minus sum of corresponding MDs after treatment at each scanning slice, divided by previous sum of MDs before treatment, multiplied by 100%. The maximal diameters of all target lesions were measured at 3D-SLICER (version 4.11, http://www.slicer.org) using CT data before DOS in transverse section with a portion of the maximal tumor extension (Figure 1) determined based on this baseline examination slice by slice. With CT data after the three cycles NAC, the maximal tumor diameters were similarly measured at the same tumor level as in the above baseline examination. For the CT evaluation before and after NAC with scan slice no greater than 5 mm, measurable lesions had to be ≥ 1 cm (long axis) for non-nodal lesions, and ≥ 1.5 cm (short

Table 1 Demographic and clinical information of all enrolled patients receiving docetaxel, oxaliplatin and S-1

Variable		Training cohort (*n* = 94)	Validation cohort (*n* = 34)
Age, yr		66.0 ± 7.0	65 ± 6.1
Gender			
	Male	77	20
	Female	17	14
cT stage			
	cT_3	62	16
	cT_4	32	18
cN stage			
	cN_0	8	3
	cN_1	36	13
	cN_2	40	14
	cN_3	10	4
Siewert type			
	II	39	18
	III	55	16
GTV (cm^3)		50.8 ± 32.0	51.1 ± 36.0

GTV: Gross tumor volume.

axis) for nodal lesions. If a lesion was non-measurable and disappeared nearly completely after NAC, it was assigned a value of 0 mm.

According to the percentage of the changes in the sum of MDs of all target lesions before and after three cycles of NAC, the responses after DOS treatment were individually divided into complete response (CR), partial response (PR), stable disease (SD) and progressive disease (PD) which were defined as follows. (1) CR: disappearance of all target lesions, confirmed at 4 wk; (2) PR: ≥ 30% decrease from baseline, confirmed at 4 wk; (3) SD: Neither PR nor PD criteria met; and (4) PD: ≥ 20% increase over smallest sum observed and overall 5-mm net increase or appearance of new lesions. Based on the above treatment responses, we used the index of disease control rate (DCR) to evaluate the response of DOS: DCR = CR + PR + SD.

Prognostic factors associated with response after DOS

Besides sex and age, the possible prognostic factors associated with responses after DOS treatment were evaluated with CT before DOS treatment. Two gastrointestinal radiologists (first author with 3 years' experience in radiology and the corresponding authors with 25 years' experience in abdominal radiology) assessed the Siewert Classification according to the tumor location, by consensus based on the portal-venous-phase-enhanced CT data[15]. AEG was divided into three types based on the distance from the epicenter of the tumor to the gastroesophageal junction (GEJ). Tumors were classified as: type I, epicenter 1–5 cm above the GEJ; type II, 1 cm above and 2 cm below the GEJ; and type III, epicenter 2–5 cm below the GEJ.

The measurement of GTV was also performed at 3D-SLICER by defining regions of interest according to the tumor area slice by slice, and we tried to avoid the air within the esophageal and gastric lumen as much as possible (Figure 1). The software automatically calculated the tumor volume. cT and cN stages before DOS determined on CT were also selected as possible prognostic factors associated with NAC response.

Inter- and intraobserver measurements of maximal tumor diameter and GTV

To ensure the accuracy of the pre and post-NAC maximal tumor diameter and pre-NAC GTV measurements in the TC and VC, two experienced radiologists (each with 3 years of radiology experience) independently measured the maximal tumor diameters and GTV to verify the interobserver repeatability. To verify intraobserver reliability, the first radiologist remeasured the maximal tumor diameters and GTV in all patients 1 month later. Before the radiologists' measurements, a radiology professor with 25 years of experience trained them how to measure the maximal tumor diameter and GTV randomly in 20 patients.

Statistical analysis

The IBM SPSS for Windows version 25.0 (SPSS, Chicago, IL, United States) was used for statistical analysis. The continuous variables were expressed as mean ± standard deviation. Categorical variables were shown as numbers and

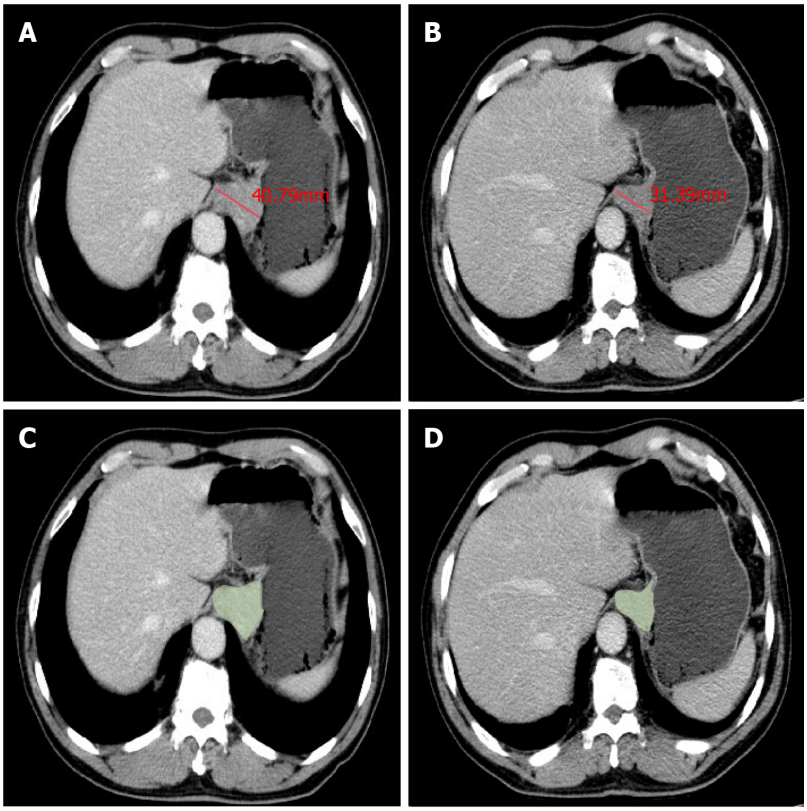

DOI: 10.4329/wjr.v16.i1.9

Figure 1 Measurements of maximal diameters and gross tumor volume based on portal venous phase contrast-enhanced computed tomography in a 65-year-old male with adenocarcinoma of the esophagogastric junction. A: Maximal diameters of the tumor before three cycles neoadjuvant chemotherapy with docetaxel, oxaliplatin and S-1 (DOS); B: Maximal diameters of the tumor after three cycles DOS; C: Gross tumor volume (GTV) of the tumor before three cycles DOS; D: GTV of the tumor after three cycles DOS.

percentages. $P < 0.05$ was considered statistically significant. The intra-class correlation coefficient (ICC) was used to evaluate the reliability of maximal tumor diameter and GTV measurements. ICC < 0.5, 0.5–0.75, 0.75–0.9, and > 0.9 was considered to have poor, moderate, good, and excellent reliability, respectively.

The χ^2 test or Fisher's test in the TC was used to assess the univariate associations of possible categorical variables with the response after NAC. The Mann–Whitney *U* test was used to determine the univariate associations of continuous variables with the response of NAC. The univariate factors with statistical significance for the response of AEG were enrolled in multivariate analysis, and binary logistic regression analysis was used to identify the independent predictors.

Establishment and validation of nomogram

The nomogram model was established based on all enrolled variables with $P < 0.05$ in multivariate analysis of the TC. The concordance index (C-index) was used to evaluate the performance of the nomogram in the two cohorts. Calibration curves were also plotted to compare nomogram-predicted DCR and actual DCR of the enrolled cohorts by using a 45-degree line as an optimal model in the two cohorts. Receiver operating characteristic (ROC) curves for the two cohorts were generated and compared based on the area under the curve (AUC). Nomogram, calibration and ROC were plotted by R4.2.1 with car, rms, pROC and rmda packages.

RESULTS

Inter- and intraobserver measurements agreements in the TC and VC

The interobserver agreements in the measurements of the pre and post-NAC maximal tumor diameter and pre-NAC GTV in the TC and VC were 0.969 [95% confidence interval (95%CI): 0.957–0.979] and 0.914 (95%CI: 0.881–0.939), respectively. The intraobserver agreements in the maximal tumor diameter and GTV measurements were 0.947 (95%CI: 0.927–0.963) and 0.982 (95%CI: 0.974–0.987), respectively. Because of all ICC values were > 0.9, the first measurements from observer 1 were repeatable, and were used for subsequent analysis.

Univariate analysis: association of prognostic factors with response after DOS in the TC

The associations of possible prognostic factors with the treatment response in AEG patients receiving DOS are shown in Table 2. Patients with Siewert type III had a greater chance to achieve DCR compared with patients with type II. Patients

Table 2 Univariate analysis of possible prognostic factors associated with responses to docetaxel, oxaliplatin and S-1

Parameter		DCR	PD	*P* value
Sex				0.664
	Male	70 (82.4)	7 (77.8)	
	Female	15 (17.6)	2 (22.2)	
Age		66.0 ± 4.1	67.2 ± 3.9	0.728
cT stage				0.028
	cT_3	57 (70.4)	5 (38.5)	
	cT_4	24 (29.6)	8 (61.5)	
cN stage				0.351
	cN_0	6 (10.2)	2 (5.7)	
	cN_1	7 (11.7)	29(82.9)	
	cN_2	37 (62.1)	3 (8.6)	
	cN_3	9 (15.2)	1 (2.8)	
Siewert type				0.005
	II	29 (35.8)	10 (76.9)	
	III	52 (64.2)	3 (23.1)	
GTV (cm^3)		47.3 ± 27.4	73.2 ± 54.3	0.040

The numbers in the parentheses are percentages. DCR: Disease control rate; PD: Progression disease; GTV: Gross tumor volume.

with cT_3 stage tumor had a greater chance to achieve DCR than those with cT_4. The larger the GTV, the poorer the response to NAC (all $P < 0.05$). However, age, gender and cN stage were not associated with treatment response (all $P > 0.05$).

Multivariate analysis: Association of factors with response after DOS in the TC

We performed logistic regression analyses to further identify potential prognostic factors for the response to DOS in the TC. Pretherapeutic cT stage ($P = 0.039$, OR = 4.631, 95%CI 1.082–14.824), GTV ($P = 0.007$, OR = 1.027, 95%CI 1.007–1.046) and Siewert type ($P = 0.014$, OR = 7.639, 95%CI 1.514–28.540) were independent prognostic factors for response to DOS.

Development and validation of nomogram model

The nomogram model (Figure 2) included three significant variables (cT stage, GTV and Siewert type) according to multivariate analysis of the TC. This model was used to predict the incidence of DCR. Each subtype of enrolled covariates including cT stage, GTV and Siewert type was assigned as a point. By adding the total points and positioning them on the bottom scale, we calculated DCR.

In the TC, the C-index of the model was 0.838 (95%CI 0.703–0.964). In the VC, the C-index of the model was 0.824 (95%CI 0.721–0.971). The predictive accuracies of the nomogram were validated in the TC and VC. The AUC of the model was 0.838 (95%CI 0.703–0.964) in the TC, and 0.824 (95%CI 0.721–0.971) in the VC (Figure 3). The calibrations curves plots performed well in the two cohorts (Figure 4).

DISCUSSION

In this study, we investigated the possible predictors associated with treatment response, and found that pretherapeutic GTV, cT stage and Siewert type as shown on CT were independent prognostic factors. We developed a nomogram model to predict the response to DOS in advanced AEG patients.

Our study demonstrated that pretherapeutic GTV could be an independent prognostic factor of AEG after DOS treatment. This finding is supported by other reports[16,17]. GTV is a comprehensive index that reflected tumor diameter and tumor invasion depth, and it has been demonstrated as a significant indicator for assessing the therapeutic response of AEG, indicating that GTV could be a prognostic factor.

As another independent prognostic factor of the response to DOS, cT stage is associated with the invasion depth of tumors, and provides prognostic estimation for clinicians. Bott *et al*[18] reported that patients with cT_3 stage esophageal adenocarcinoma were more likely to achieve DCR than those with cT_4 stage, illustrating that cT stage can be an effective index to predict treatment prognosis. This finding can be explained by a high expression level of special AT-rich binding

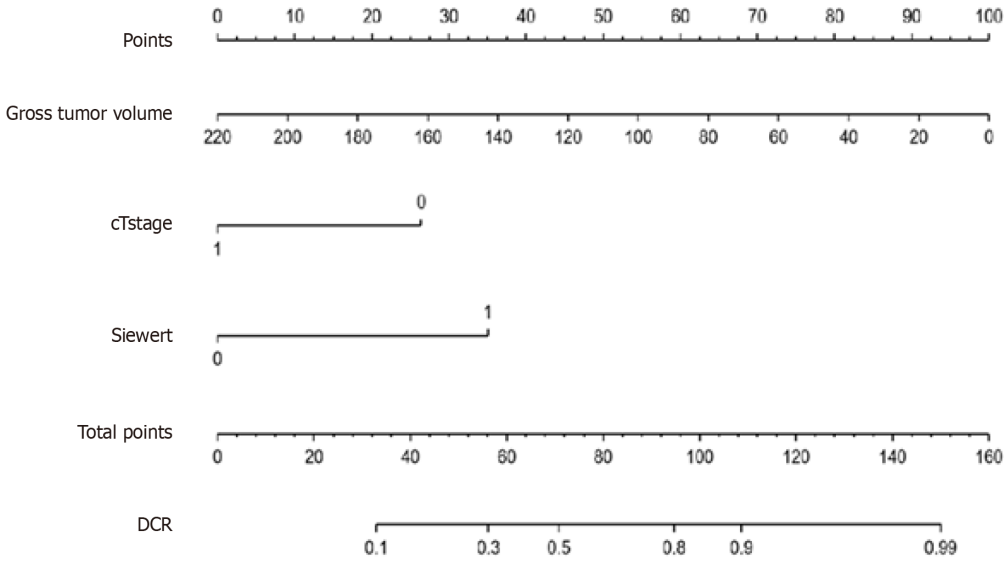

DOI: 10.4329/wjr.v16.i1.9 **Copyright** ©The Author(s) 2024.

Figure 2 Nomogram was developed to predict disease control rate of adenocarcinoma of the esophagogastric junction after three cycles of neoadjuvant chemotherapy with docetaxel, oxaliplatin and S-1. DCR: Disease control rate.

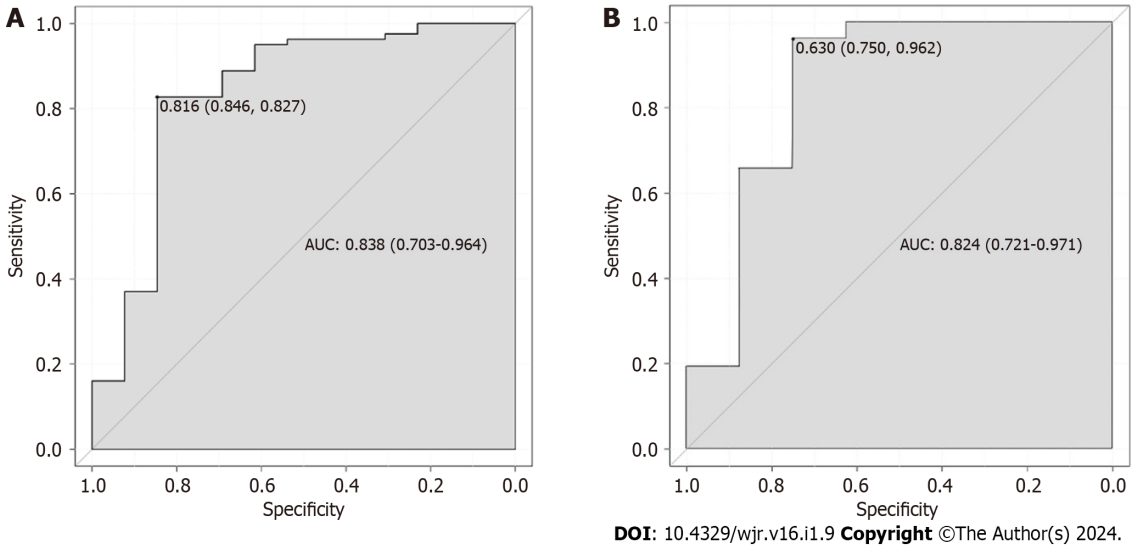

DOI: 10.4329/wjr.v16.i1.9 **Copyright** ©The Author(s) 2024.

Figure 3 Receiver operating characteristic curves of the nomogram. A: Area under curve with 0.838 in training cohort; B: Area under curve with 0.824 in validation cohort.

protein 1 in patients with cT_4 stage gastric cancer, which plays a vital role in facilitating tumor invasion, metastasis and multidrug resistance, resulting in the unsatisfactory response in tumors with later cT stage[19-21].

Our study demonstrated that patients with Siewert type III AEG could benefit more from DOS than patients with type II. Studies have shown the histological differences between types II and III AEG. Compared with patients with type II AEG, background mucosa of patients with type III mainly showed moderate to marked atrophy and intestinal metaplasia, and almost half of type II AEG originated from gastritis-unrelated mucosa[22,23]. AEGs with atrophy or intestinal metaplasia were less aggressive than those without these histological changes, and the prognosis of tumors with intestinal metaplasia was better than of tumors without intestinal metaplasia. Besides, AEG with atrophy or intestinal metaplasia benefited more from NAC compared with the diffuse type[7,24].

Clinically, we established a novel nomogram based on pretherapeutic cT stage, Siewert type and GTV to predict the response of DOS in patients with AEG, and the C-indexes of the models in the TC and VC were 0.838 and 0.824, respectively, suggesting good predictive ability. By identifying non-responders, the treatment strategies for these patients may be adjusted accordingly; therefore, these patients could avoid the adverse effects associated with NAC and thus prolong their survival.

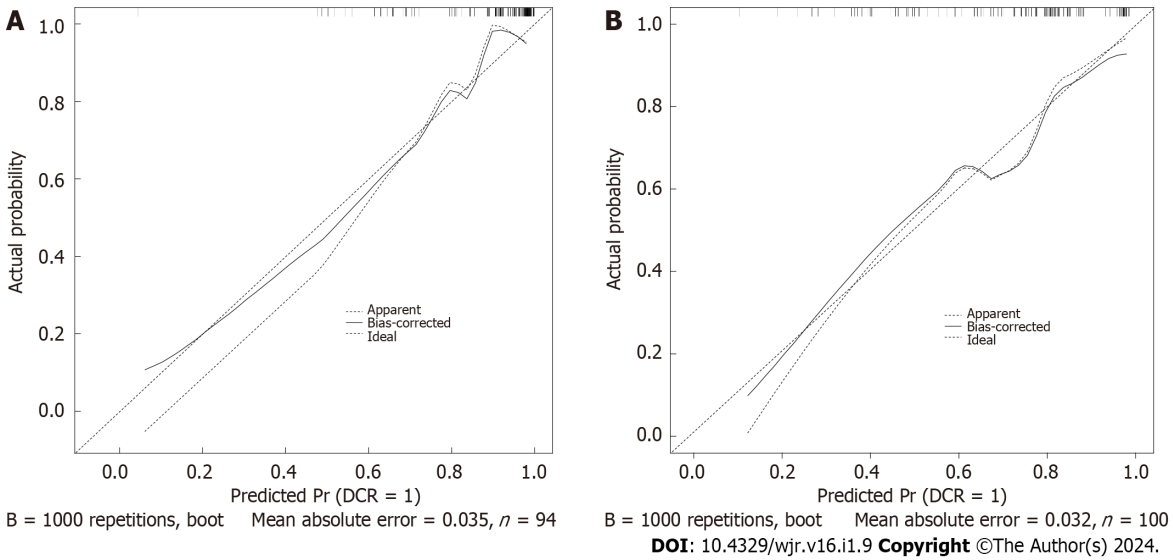

DOI: 10.4329/wjr.v16.i1.9

Figure 4 Calibration curve of the nomogram. A: Calibration curve in the training cohort; B: Calibration curve in the validation cohort.

The study had some limitations. First, this was a single-center study, indicating that the general applicability of our model needs further validation. Second, the sample size was small, especially for patients with CR. Our model still showed excellent performance. In the future, we will expand the sample size for further study.

CONCLUSION

In conclusion, this study illustrated that pretherapeutic cT stage, GTV and Siewert type could be independent prognostic factors for response to DOS. Based on the three independent prognostic factors, a novel nomogram was established to predict the response to DOS. We hope that our nomogram will help clinicians select suitable patients with Siewert types II and III AEG to undergo DOS, and identify non-responders to adjust the treatment strategies and to avoid toxicity associated with DOS.

ARTICLE HIGHLIGHTS

Research background

The incidence of adenocarcinoma of esophagogastric junction (AEG) has increased worldwide, and the survival rate is unsatisfactory. Generally, most patients are diagnosed in the advanced stage. Multimodal treatment has become the standard of care for locally advanced AEG. The NAC regimen for AEG patients differ regionally. Some research has indicated superiority of a docetaxel-based regimen over the established regimens, including S-1 and oxaliplatin, and cisplatin and fluorouracil. The Eastern Asia countries mostly used docetaxel, oxaliplatin and S-1 (DOS) as first-line NAC. However, research has demonstrated that patients who do not respond to DOS have a significantly worse prognosis. For docetaxel-based regimens, the key is to select AEG patients who optimally benefit from DOS and who do not respond to DOS in clinical practice.

Research motivation

The optimal treatment choice for AEG relies on the TNM staging and anatomical location. To evaluate the TNM stage and location, endoscopic ultrasound and computed tomography (CT) are the most common choices at present. Compared with endoscopic ultrasound, CT can clearly show the morphological characteristics of the tumor, in addition to cT stage, cN stage and location of the lesion, and can measure tumor diameter and volume to assess the response to NAC. To our knowledge, there is no report on the development of a model based on CT characteristics to predict the response to DOS for advanced AEG patients.

Research objectives

Our study aimed to establish and validate a novel nomogram based on CT characteristics to predict response to DOS, which could be helpful to choose optimal treatment and avoid the toxicity of DOS.

Research methods

One hundred and twenty-eight consecutive patients with confirmed Siewert type II/III AEG underwent CT before and

after three cycles of NAC with DOS, and were randomly and consecutively assigned to the training cohort (TC) (n = 94) and the validation cohort (VC) (n = 34). Therapeutic effect was assessed by disease-control rate and progressive disease according to the Response Evaluation Criteria in Solid Tumors (version 1.1) criteria. Possible prognostic factors associated with responses after DOS treatment including Siewert classification, gross tumor volume (GTV), and cT and cN stages were evaluated using pretherapeutic CT data in addition to sex and age. Univariate and multivariate analyses of CT and clinical features in the TC were performed to determine independent factors associated with response to DOS. A nomogram was established based on independent factors to predict the response. The predictive performance of the nomogram was evaluated by Concordance index (C-index), calibration and receiver operating characteristics curve in the TC and VC.

Research results

Univariate analysis showed that Siewert type (52/55 *vs* 29/39, P = 0.005), pretherapeutic cT stage (57/62 *vs* 24/32, P = 0.028), GTV (47.3 ± 27.4 *vs* 73.2 ± 54.3, P = 0.040) were significantly associated with response to DOS in the TC. Multivariate analysis of the TC also showed that the pretherapeutic cT stage, GTV and Siewert type were independent predictive factors related to response to DOS (odds ratio = 4.631, 1.027 and 7.639, respectively; all P < 0.05). The nomogram developed with these independent factors showed an excellent performance to predict response to DOS in the TC and VC (C-index: 0.838 and 0.824), with area under the receiver operating characteristic curve of 0.838 and 0.824, respectively. The calibration curves showed that the practical and predicted response to DOS effectively coincided.

Research conclusions

This study illustrated that pretherapeutic cT stage, GTV and Siewert type could be independent prognostic factors for response to DOS. Based on the three independent prognostic factors, a novel nomogram was established to predict the response to DOS.

Research perspectives

We have developed a novel nomogram based on the independent prognostic factors including pretherapeutic cT stage, GTV and Siewert type of AEG as depicted on CT to predict response to DOS. We hope that our nomogram will help clinicians select suitable patients with Siewert types II and III AEG to undergo DOS, and identify non-responders to adjust the treatment strategies and to avoid toxicity associated with DOS.

FOOTNOTES

Co-first authors: Chuan-Qinyuan Zhou and Dan Gao.

Author contributions: Chen TW, Gui Y and Zhang XM proposed the study; Zhou CQ, Gao D, Li NP, Guo WW, Zhou HY, Li R and Chen J performed the research and collected the data; Zhou CQ was responsible for patient screening, enrollment, collection of clinical and image data; Zhou CQ and Gao D measured the diameter of tumor, and Gao D divided the subjects according to the diameter changes of tumor; both authors have made crucial and indispensable contributions towards the completion of the project and thus qualified as the co-first authors of the paper; Zhou CQ and Chen TW analyzed the data and wrote the first draft; all authors contributed to the interpretation of the study and to further drafts; all authors read and approved the final manuscript; Chen TW is the guarantor.

Supported by the National Natural Science Foundation of China, No. 82271959, and the Nanchong-University Cooperative Research Project, No. 20SXQT0329.

Institutional review board statement: The study was reviewed and approved by the (Affiliated Hospital of North Sichuan Medical College) Institutional Review Board [(Approval No. 2023ER335-1)].

Informed consent statement: All study participants or their legal guardian provided informed written consent about personal and medical data collection prior to study enrolment.

Conflict-of-interest statement: There are no conflicts of interest to declare in this study.

Data sharing statement: Please contact the corresponding author for data requests.

STROBE statement: The authors have read the STROBE Statement—checklist of items, and the manuscript was prepared and revised according to the STROBE Statement—checklist of items.

Country/Territory of origin: China

ORCID number: Chuan-Qinyuan Zhou 0009-0007-9157-4577; Tian-Wu Chen 0000-0001-5776-3429.

S-Editor: Liu JH
L-Editor: A
P-Editor: Zhao S

REFERENCES

1 **Chevallay M**, Bollschweiler E, Chandramohan SM, Schmidt T, Koch O, Demanzoni G, Mönig S, Allum W. Cancer of the gastroesophageal junction: a diagnosis, classification, and management review. *Ann N Y Acad Sci* 2018; **1434**: 132-138 [PMID: 30138540 DOI: 10.1111/nyas.13954]
2 **Rice TW**, Ishwaran H, Ferguson MK, Blackstone EH, Goldstraw P. Cancer of the Esophagus and Esophagogastric Junction: An Eighth Edition Staging Primer. *J Thorac Oncol* 2017; **12**: 36-42 [PMID: 27810391 DOI: 10.1016/j.jtho.2016.10.016]
3 **Jung MK**, Schmidt T, Chon SH, Chevallay M, Berlth F, Akiyama J, Gutschow CA, Mönig SP. Current surgical treatment standards for esophageal and esophagogastric junction cancer. *Ann N Y Acad Sci* 2020; **1482**: 77-84 [PMID: 32798235 DOI: 10.1111/nyas.14454]
4 **Eyck BM**, van Lanschot JJB, Hulshof MCCM, van der Wilk BJ, Shapiro J, van Hagen P, van Berge Henegouwen MI, Wijnhoven BPL, van Laarhoven HWM, Nieuwenhuijzen GAP, Hospers GAP, Bonenkamp JJ, Cuesta MA, Blaisse RJB, Busch OR, Creemers GM, Punt CJA, Plukker JTM, Verheul HMW, Spillenaar Bilgen EJ, van der Sangen MJC, Rozema T, Ten Kate FJW, Beukema JC, Piet AHM, van Rij CM, Reinders JG, Tilanus HW, Steyerberg EW, van der Gaast A; CROSS Study Group. Ten-Year Outcome of Neoadjuvant Chemoradiotherapy Plus Surgery for Esophageal Cancer: The Randomized Controlled CROSS Trial. *J Clin Oncol* 2021; **39**: 1995-2004 [PMID: 33891478 DOI: 10.1200/JCO.20.03614]
5 **Bang YJ**, Kim YW, Yang HK, Chung HC, Park YK, Lee KH, Lee KW, Kim YH, Noh SI, Cho JY, Mok YJ, Ji J, Yeh TS, Button P, Sirzén F, Noh SH; CLASSIC trial investigators. Adjuvant capecitabine and oxaliplatin for gastric cancer after D2 gastrectomy (CLASSIC): a phase 3 open-label, randomised controlled trial. *Lancet* 2012; **379**: 315-321 [PMID: 22226517 DOI: 10.1016/S0140-6736(11)61873-4]
6 **Saito T**, Kurokawa Y, Takahashi T, Yamamoto K, Yamashita K, Tanaka K, Makino T, Nakajima K, Eguchi H, Doki Y. Neoadjuvant docetaxel, oxaliplatin and S1 (DOS) combination chemotherapy for patients with resectable adenocarcinoma of esophagogastric junction. *Gastric Cancer* 2022; **25**: 966-972 [PMID: 35488968 DOI: 10.1007/s10120-022-01300-1]
7 **Al-Batran SE**, Hofheinz RD, Pauligk C, Kopp HG, Haag GM, Luley KB, Meiler J, Homann N, Lorenzen S, Schmalenberg H, Probst S, Koenigsmann M, Egger M, Prasnikar N, Caca K, Trojan J, Martens UM, Block A, Fischbach W, Mahlberg R, Clemens M, Illerhaus G, Zirlik K, Behringer DM, Schmiegel W, Pohl M, Heike M, Ronellenfitsch U, Schuler M, Bechstein WO, Königsrainer A, Gaiser T, Schirmacher P, Hozaeel W, Reichart A, Goetze TO, Sievert M, Jäger E, Mönig S, Tannapfel A. Histopathological regression after neoadjuvant docetaxel, oxaliplatin, fluorouracil, and leucovorin *vs* epirubicin, cisplatin, and fluorouracil or capecitabine in patients with resectable gastric or gastro-oesophageal junction adenocarcinoma (FLOT4-AIO): results from the phase 2 part of a multicentre, open-label, randomised phase 2/3 trial. *Lancet Oncol* 2016; **17**: 1697-1708 [PMID: 27776843 DOI: 10.1016/S1470-2045(16)30531-9]
8 **Dos Santos M**, Lequesne J, Leconte A, Corbinais S, Parzy A, Guilloit JM, Varatharajah S, Brachet PE, Dorbeau M, Vaur D, Weiswald LB, Poulain L, Le Gallic C, Castera-Tellier M, Galais MP, Clarisse B. Perioperative treatment in resectable gastric cancer with spartalizumab in combination with fluorouracil, leucovorin, oxaliplatin and docetaxel (FLOT): a phase II study (GASPAR). *BMC Cancer* 2022; **22**: 537 [PMID: 35549674 DOI: 10.1186/s12885-022-09623-z]
9 **Räsänen JV**, Sihvo EI, Knuuti MJ, Minn HR, Luostarinen ME, Laippala P, Viljanen T, Salo JA. Prospective analysis of accuracy of positron emission tomography, computed tomography, and endoscopic ultrasonography in staging of adenocarcinoma of the esophagus and the esophagogastric junction. *Ann Surg Oncol* 2003; **10**: 954-960 [PMID: 14527917 DOI: 10.1245/aso.2003.12.002]
10 **Parry K**, Haverkamp L, Bruijnen RC, Siersema PD, Offerhaus GJ, Ruurda JP, van Hillegersberg R. Staging of adenocarcinoma of the gastroesophageal junction. *Eur J Surg Oncol* 2016; **42**: 400-406 [PMID: 26777127 DOI: 10.1016/j.ejso.2015.11.014]
11 **Beer AJ**, Wieder HA, Lordick F, Ott K, Fischer M, Becker K, Stollfuss J, Rummeny EJ. Adenocarcinomas of esophagogastric junction: multi-detector row CT to evaluate early response to neoadjuvant chemotherapy. *Radiology* 2006; **239**: 472-480 [PMID: 16543584 DOI: 10.1148/radiol.2391050043]
12 **Hofheinz RD**, Hegewisch-Becker S, Kunzmann V, Thuss-Patience P, Fuchs M, Homann N, Graeven U, Schulte N, Merx K, Pohl M, Held S, Keller R, Tannapfel A, Al-Batran SE. Trastuzumab in combination with 5-fluorouracil, leucovorin, oxaliplatin and docetaxel as perioperative treatment for patients with human epidermal growth factor receptor 2-positive locally advanced esophagogastric adenocarcinoma: A phase II trial of the Arbeitsgemeinschaft Internistische Onkologie Gastric Cancer Study Group. *Int J Cancer* 2021; **149**: 1322-1331 [PMID: 34019698 DOI: 10.1002/ijc.33696]
13 **Ajani JA**, D'Amico TA, Bentrem DJ, Chao J, Corvera C, Das P, Denlinger CS, Enzinger PC, Fanta P, Farjah F, Gerdes H, Gibson M, Glasgow RE, Hayman JA, Hochwald S, Hofstetter WL, Ilson DH, Jaroszewski D, Johung KL, Keswani RN, Kleinberg LR, Leong S, Ly QP, Matkowskyj KA, McNamara M, Mulcahy MF, Paluri RK, Park H, Perry KA, Pimiento J, Poultsides GA, Roses R, Strong VE, Wiesner G, Willett CG, Wright CD, McMillian NR, Pluchino LA. Esophageal and Esophagogastric Junction Cancers, Version 2.2019, NCCN Clinical Practice Guidelines in Oncology. *J Natl Compr Canc Netw* 2019; **17**: 855-883 [PMID: 31319389 DOI: 10.6004/jnccn.2019.0033]
14 **Iannessi A**, Beaumont H, Liu Y, Bertrand AS. RECIST 1.1 and lesion selection: How to deal with ambiguity at baseline? *Insights Imaging* 2021; **12**: 36 [PMID: 33738548 DOI: 10.1186/s13244-021-00976-w]
15 **Wang J**, Zhong L, Zhou X, Chen D, Li R. Value of multiphase contrast-enhanced CT with three-dimensional reconstruction in detecting depth of infiltration, lymph node metastasis, and extramural vascular invasion of gastric cancer. *J Gastrointest Oncol* 2021; **12**: 1351-1362 [PMID: 34532093 DOI: 10.21037/jgo-21-276]
16 **Tang X**, He Q, Qu H, Sun G, Liu J, Gao L, Shi J, Ye J, Liang Y. Post-therapy pathologic tumor volume predicts survival in gastric cancer patients who underwent neoadjuvant chemotherapy and gastrectomy. *BMC Cancer* 2019; **19**: 797 [PMID: 31409315 DOI: 10.1186/s12885-019-6012-7]
17 **Li R**, Chen TW, Hu J, Guo DD, Zhang XM, Deng D, Li H, Chen XL, Tang HJ. Tumor volume of resectable adenocarcinoma of the esophagogastric junction at multidetector CT: association with regional lymph node metastasis and N stage. *Radiology* 2013; **269**: 130-138 [PMID: 23657894 DOI: 10.1148/radiol.13122269]
18 **Bott RK**, George G, McEwen R, Zylstra J, Knight WRC, Baker CR, Kelly M, Griffin N, McAddy N, Maisey N, Van Hemelrijck M, Gossage

JA, Lagergren J, Davies AR. Predicting response to neoadjuvant chemotherapy in patients with oesophageal adenocarcinoma. *Acta Oncol* 2021; **60**: 1629-1636 [PMID: 34613874 DOI: 10.1080/0284186X.2021.1986228]

19 **Glatzel-Plucińska N**, Piotrowska A, Dzięgiel P, Podhorska-Okołów M. The Role of SATB1 in Tumour Progression and Metastasis. *Int J Mol Sci* 2019; **20** [PMID: 31450715 DOI: 10.3390/ijms20174156]

20 **Smolińska M**, Grzanka D, Antosik P, Kasperska A, Neska-Długosz I, Jóźwicki J, Klimaszewska-Wiśniewska A. HER2, NF-κB, and SATB1 Expression Patterns in Gastric Cancer and Their Correlation with Clinical and Pathological Parameters. *Dis Markers* 2019; **2019**: 6315936 [PMID: 31737131 DOI: 10.1155/2019/6315936]

21 **Jenke R**, Holzhäuser-Rein M, Mueller-Wilke S, Lordick F, Aigner A, Büch T. SATB1-Mediated Upregulation of the Oncogenic Receptor Tyrosine Kinase HER3 Antagonizes MET Inhibition in Gastric Cancer Cells. *Int J Mol Sci* 2020; **22** [PMID: 33374770 DOI: 10.3390/ijms22010082]

22 **Urabe M**, Ushiku T, Shinozaki-Ushiku A, Iwasaki A, Yamazawa S, Yamashita H, Seto Y, Fukayama M. Adenocarcinoma of the esophagogastric junction and its background mucosal pathology: A comparative analysis according to Siewert classification in a Japanese cohort. *Cancer Med* 2018; **7**: 5145-5154 [PMID: 30239168 DOI: 10.1002/cam4.1763]

23 **Kumamoto T**, Kurahashi Y, Niwa H, Nakanishi Y, Okumura K, Ozawa R, Ishida Y, Shinohara H. True esophagogastric junction adenocarcinoma: background of its definition and current surgical trends. *Surg Today* 2020; **50**: 809-814 [PMID: 31278583 DOI: 10.1007/s00595-019-01843-4]

24 **Zhou D**, Ye C, Pan Z, Deng Y. SATB1 Knockdown Inhibits Proliferation and Invasion and Decreases Chemoradiation Resistance in Nasopharyngeal Carcinoma Cells by Reversing EMT and Suppressing MMP-9. *Int J Med Sci* 2021; **18**: 42-52 [PMID: 33390772 DOI: 10.7150/ijms.49792]

World Journal of Radiology

Submit a Manuscript: https://www.f6publishing.com

World J Radiol 2024 January 28; 16(1): 20-31

DOI: 10.4329/wjr.v16.i1.20

ISSN 1949-8470 (online)

SYSTEMATIC REVIEWS

From strength to precision: A systematic review exploring the clinical utility of 7-Tesla magnetic resonance imaging in abdominal imaging

Arosh S Perera Molligoda Arachchige, Ana Claudia Teixeira de Castro Gonçalves Ortega, Federica Catapano, Letterio S Politi, Michael N Hoff

Specialty type: Radiology, nuclear medicine and medical imaging

Provenance and peer review: Invited article; Externally peer reviewed.

Peer-review model: Single blind

Peer-review report's scientific quality classification

Grade A (Excellent): 0
Grade B (Very good): 0
Grade C (Good): C
Grade D (Fair): 0
Grade E (Poor): 0

P-Reviewer: Alzerwi NAN, Saudi Arabia

Received: October 16, 2023
Peer-review started: October 16, 2023
First decision: November 9, 2023
Revised: December 6, 2023
Accepted: December 25, 2023
Article in press: December 25, 2023
Published online: January 28, 2024

Arosh S Perera Molligoda Arachchige, Ana Claudia Teixeira de Castro Gonçalves Ortega, Faculty of Medicine, Humanitas University, Pieve Emanuele 20072, Milan, Italy

Federica Catapano, Letterio S Politi, Department of Biomedical Sciences, Humanitas University, Pieve Emanuele 20072, Milan, Italy

Federica Catapano, IRCCS Humanitas Research Hospital, Rozzano 20089, Milan, Italy

Letterio S Politi, Department of Neuroradiology, IRCCS Humanitas Research Hospital, Rozzano 20089, Milan, Italy

Michael N Hoff, Department of Radiology and Biomedical Imaging, University of California, San Francisco, CA 94143, United States

Corresponding author: Michael N Hoff, PhD, Professor, Department of Radiology and Biomedical Imaging, University of California, San Francisco, 505 Parnassus Ave, San Francisco, California CA 94143, United States. michael.hoff2@ucsf.edu

Abstract

BACKGROUND

After approval for clinical use in 2017 early investigations of ultra-high-field abdominal magnetic resonance imaging (MRI) have demonstrated the feasibility as well as diagnostic capabilities of liver, kidney, and prostate MRI at 7-Tesla. However, the elevation of the field strength to 7-Tesla not only brought advantages to abdominal MRI but also presented considerable challenges and drawbacks, primarily stemming from heightened artifacts and limitations in Specific Absorption Rate, *etc.* Furthermore, evidence in the literature is relatively scarce concerning human studies in comparison to phantom/animal studies which necessitates an investigation into the evidence so far in humans and summarizing all relevant evidence.

AIM

To offer a comprehensive overview of current literature on clinical abdominal 7T MRI that emphasizes current trends, details relevant challenges, and provides a concise set of potential solutions.

METHODS

This systematic review adheres to Preferred Reporting Items for Systematic Reviews and Meta-Analyses guidelines. A PubMed search, utilizing Medical Subject Headings terms such as "7-Tesla" and organ-specific terms, was conducted for articles published between January 1, 1985, and July 25, 2023. Eligibility criteria included studies exploring 7T MRI for imaging human abdominal organs, encompassing various study types (*in-vivo*/*ex-vivo*, method development, reviews/meta-analyses). Exclusion criteria involved animal studies and those lacking extractable data. Study selection involved initial identification *via* title/abstract, followed by a full-text review by two researchers, with discrepancies resolved through discussion. Data extraction covered publication details, study design, population, sample size, 7T MRI protocol, image characteristics, endpoints, and conclusions.

RESULTS

The systematic review included a total of 21 studies. The distribution of clinical 7T abdominal imaging studies revealed a predominant focus on the prostate (n = 8), followed by the kidney (n = 6) and the hepatobiliary system (n = 5). Studies on these organs, and in the pancreas, demonstrated clear advantages at 7T. However, small bowel studies showed no significant improvements compared to traditional MRI at 1.5T. The majority of studies evaluated originated from Germany (n = 10), followed by the Netherlands (n = 5), the United States (n = 5), Austria (n = 2), the United Kingdom (n = 1), and Italy (n = 1).

CONCLUSION

Further increase of abdominal clinical MRI field strength to 7T demonstrated high imaging potential, yet also limitations mainly due to the inhomogeneous radiofrequency (RF) excitation field relative to lower field strengths. Hence, further optimization of dedicated RF coil elements and pulse sequences are expected to better optimize clinical imaging at high magnetic field strength.

Key Words: 7-Tesla magnetic resonance imaging; Abdominal; Prostate; Kidney; Renal; Pancreas; Hepatobiliary; Liver; Small bowel

Core Tip: At 7T non-enhanced T1w imaging, especially time-of-flight magnetic resonance angiography, excels in liver vessel assessment, outperforming both steady-state free precession and T2-weighted TSE techniques. Additionally, 7T magnetic resonance spectroscopy (MRS), particularly 31P-MRS, provides valuable insights into hepatic energy metabolism in non-alcoholic fatty liver disease/non-alcoholic steatohepatitis. In pancreatic evaluation, 7T magnetic resonance imaging (MRI) holds promise for tumor characterization. Renal 7T MRI demonstrates potential for reducing contrast use, and prostate imaging explores metabolomic profiles and multi-voxel MRS for cancer detection. Imaging the small bowel at 7T currently offers no significant advantages. Despite challenges 7T MRI holds promise for advancing abdominal diagnostics.

Citation: Perera Molligoda Arachchige AS, Teixeira de Castro Gonçalves Ortega AC, Catapano F, Politi LS, Hoff MN. From strength to precision: A systematic review exploring the clinical utility of 7-Tesla magnetic resonance imaging in abdominal imaging. *World J Radiol* 2024; 16(1): 20-31

URL: https://www.wjgnet.com/1949-8470/full/v16/i1/20.htm

DOI: https://dx.doi.org/10.4329/wjr.v16.i1.20

INTRODUCTION

Magnetic resonance imaging (MRI) of the abdomen is a proven and useful tool for the evaluation, assessment of severity, and follow-up of diseases of the abdomen as summarized by the American College of Radiology[1]. It is an evolving technology involving a variety of pulse sequences and protocols that are continuously being modified and improved.

It is well-known that unlike traditional X-rays, standard clinical MRI relies on the behaviour of hydrogen protons in response to these magnetic fields. Higher MRI magnetic field strengths ensure that more protons align with the field, generating more usable tissue magnetization. This enhances image signal relative to background noise. Initially, scientists believed 0.5T would be the maximum clinical magnet strength due to concerns about radiofrequency penetration in live tissue[2]. However, 1.5T clinical scanners started becoming available in the 1980s, and by 2002, 3T scanners gained approval. Although the first 7T research scanners emerged in 1999, they were limited to neuroimaging and some extremity applications. The first body images showcasing potential for prostate imaging at 7T were presented in 2007. Motivated by the desire to enhance resolution and contrast, 7T body MRI expanded, with the first abdominal images published in 2009. Today, 7T MRI is even employed in imaging challenging anatomical regions such as cardiac tissue[3]. Although multiple groups have worked on developing 7T methods and overcoming associated challenges, it wasn't until 2017 that 7T scanners received United States Food and Drug Administration and European Medicines Agency approval

for clinical use[4]. Since then, there has been growth of *in vivo* body applications of 7T MRI in humans. Initial efforts involved acquiring landscaping image sets to establish the overall feasibility and safety of 7T whole body, breast, cardiac and metabolic magnetic resonance (MR) imaging. Subsequent publications have shifted focus towards implementing standardized imaging protocols to explore the diagnostic capacity of 7T abdominal MRI in dedicated examinations of non-enhanced and contrast-enhanced liver and kidney imaging, as well as renal MR angiographic applications[5-9]. This systematic review aims to provide an overview of the work currently published on clinical abdominal 7T MRI, where challenges to its application will be detailed along with a short overview of possible solutions.

MATERIALS AND METHODS

Search strategy

The systematic review follows the guidelines of the Preferred Reporting Items for Systematic Reviews and Meta-Analyses (PRISMA) statement. We used the PubMed database to perform the literature search using the following MeSH terms: "7-Tesla" AND "abdominal" OR "renal" OR "kidney" OR "pancreas" OR "pancreatitis" OR "pancreatic" OR "liver" OR "hepatic" OR "hepatobiliary" OR "spleen" OR "intestine" OR "colon" OR "bladder" OR "uterus" OR "ovaries" OR "prostate". Articles published between January 1, 1985 to July 25, 2023 were searched.

Eligibility criteria

Studies were included that investigated the use of 7T MRI for any human abdominal organ and their associated disorders. In particular, studies were included if they were: (1) Human studies; (2) *in-vivo*/post-mortem/histological/*ex-vivo* studies; (3) related to MRI sequence/method development; and/or (4) reviews/case series or meta-analyses. Studies were excluded if they were: (1) Animal studies; (2) simulations; or (3) yielded no extractable data.

Study selection

Studies were first identified by a single researcher through review of titles/abstracts. Any study that used 7T MRI to investigate the abdominal organs and disorders was moved to the next stage of screening. The second round of screening was conducted by two researchers based on the full text, following the eligibility criteria mentioned above. Any discrepancies in judgment were resolved through discussion.

Data extraction

The following data were extracted: publication characteristics (first author and year of publication), study design, study population, sample size, 7T MRI protocol, imaging protocol/characteristics, endpoints, and conclusions.

RESULTS

Studies reviewed

The search strategy produced 158 results, amongst which 62 studies were screened by title/abstract to yield 38 studies for further full-text review. Finally, after filtering by eligibility criteria, data extraction for qualitative synthesis was conducted on 21 studies *via* manual citation review (Figure 1)[10].

Risk of bias assessment

We used Version 2 of the Cochrane risk-of-bias tool for randomized trials (RoB 2.0) to obtain the Traffic-Light plot for the risk of bias assessment for all original investigative studies[11]. The risk of bias was initially evaluated by one researcher, everything was reviewed by the second researcher, and any disagreements were discussed before arriving at a conclusion. Risk of bias was assessed across five domains D1-D5, with D1 being the bias due to randomization, D2 being bias due to deviation from intended intervention, D3 being bias due to missing outcome data, D4 being bias in the measurement of outcome, and D5 being bias during the selection of the reported result, see Figure 2.

Distribution of clinical 7T abdominal imaging studies

The focus on the studies were predominantly on the prostate (n = 8), followed by the kidney (n = 6) and the hepatobiliary system (n = 5). While the studies on the prostate, kidney, hepatobiliary system, and pancreas demonstrated clear advantages at 7T, small bowel studies showed no significant improvements relative to traditional MRI (1.5 T). The largest number of studies are reported from Germany (n = 10) followed by the Netherlands (n = 5), the United States (n = 5), Austria (n = 2), United Kingdom (n = 1), Italy (n = 1), see Figure 3.

Techniques and protocols for 7T abdominal MRI

Overall, 22 studies have been summarized in Table 1 with details on study design, imaging protocols, study sample, and endpoints/applications. Note that the study by Tenbergen *et al*[12] is not included in the table since we only included original investigations.

Table 1 Overview of studies evaluating abdominal organs with 7T-magnetic resonance imaging

Ref.	Study Design	MRI model, RF Coil & Imaging Parameters	No. of patients	Endpoints/Applications
Fischer *et al* [17], 2014	Prospective study	Siemens Terra: 8-channel transmit/receive body coil; T1w 2D FLASH TOF MRA; transversal orientation; TR = 17ms; TE = 4.7 ms; TA = 0:33 s	12	For non-enhanced MR imaging of the arterial, venous and portal liver vessels in candidates for hepatectomy or liver transplantation with acute or chronic renal insufficiency
Traussnigg *et al* [20], 2017	Prospective Non-randomized feasibility study	Siemens Terra; surface coil (1H/31P, 10 cm diameter, Rapid Biomedical GmbH), 2D 31P-MR CSI sequence, TA = approximately 10 min	30	As a non-invasive tool for obtaining pathomechanistic insights to improve risk stratification using changes in energy metabolism including dynamic ATP flux in inflammation and fibrosis in non-alcoholic fatty liver disease (NAFLD) and steato-hepatitis (NASH)
Beiderwellen *et al*[28], 2017	Prospective study	Siemens Terra; 8-channel transmit/receive body coil; T1w 3D spoiled gradient-echo VIBE sequence; coronal; post-contrast; TR = 2.90 ms; TE = 1.09 ms; TA = 27s; Resolution = 1.25 mm × 1.25 mm × 1.6 mm	10	For Gadobutrol dose reduction (to 0.025 mmol/kg of body weight) while maintaining diagnostic image quality for the diagnosis of renal artery stenosis in patients with renal impairment
Purvis *et al*[21], 2017	Prospective study	Siemens Terra; 16-channel 31P RF array heart/liver butterfly-loop coil pair; 3D UTE CSI sequence; TA = approximately 28 min	26	For studying metabolism in liver disease
Wu *et al*[30], 2010	Pilot study (*ex-vivo*)	Siemens Terra; T2w TSE and PRESS with CHESS water suppression; TE/TR = 30/1700 ms; resolution = 3 mm^3 isotropic; TA = approximately 23 min; MRS data processed using NMR Software Nuts (Acorn NMR Inc., Livermore, CA, United States)	N/A	To construct a malignancy index based on prostate cancer metabolomic profiles
Rosenkrantz *et al*[33], 2015	Feasibility study	Siemens Terra: Axial TSE T2w sequence; TR = 11670 ms; TE = 80 ms; FA = 160; Resolution = 0.75 mm × 0.75 mm × 3 mm; BW 254 Hz/voxel; NEX = 1	3	For tumor localization using T2w MRI at 7T before prostatectomy
Luttje *et al*[32], 2014	Feasibility study	Siemens Terra: 2D 1H MRSI grid positioned in the tumor location as seen, 3D 31P MRSI grid positioned over whole prostate; TE/TR = 56/2000 ms; resolution = 5 mm × 5 mm × 5 mm; TA = 448s; 3D 31P MRSI TE/TR = 0.42/200 ms; FA = 20°, resolution = 12 mm × 12 mm × 12 mm, TA = 610s	5	To acquire both 1H and 31P MRS within the same scan session in patients with prostate cancer
Lagemaat *et al* [35], 2015	Prospective study	B0 and B1+ field-mapping to optimize B0 and B1 field homogeneity in the prostate; T2wTE = 71 ms; TR = 3000–3640 ms; resolution 0.75 mm × 0.75 mm × 3 mm with overlaid 2D 31P T1 3D 31P MRSI Nuclear Overhauser Effect (NOE) measurements	12	Optimization of phosphorus (31P) MRSI of the human prostate at 7 T by the evaluation of T1 relaxation times and the NOE of phosphorus-containing metabolites
Vos *et al*[31], 2014	Prospective study	Siemens Terra; 8-channel TxRx body array coil + an endorectal coil tuned to the P31 frequency; Axial/sagittal T2w FSE TR = 3000/3640 ms; TA = 90/113s	17	Prostate cancer is visualized on T2-weighted MRI with periprostatic lipids appearing hypo-intense compared to healthy peripheral zone tissue
Durand *et al* [34], 2017	Feasibility study (*ex-vivo*)		N/A	To determine high-resolution *ex-vivo* MRI protocol parameters for characterization of prostate tissue at histological length scales
Philips *et al* [36], 2019	Pilot study	Siemens Terra; Combined 31P Tx/Rx and 1H Rx endorectal coil (31P/ 1H ERC), 8-channel external multitransmit 1H array; T2w TSE, resolution 0.43 mm × 0.43 mm × 3 mm; TA = 119s; DWI EPI (RESOLVE) b0, b100, b400, and b800, resolution 1.75 mm × 1.75 mm × 3 mm, TA = 274s; 31P 3D MRSI with non-selective BIR-4 excitation, TA = 789s; 1H MRSI PRESS TA = 421s	4	To perform high resolution multiparametric MR imaging and 1H and 31P spectroscopy of the prostate using a 31P Tx/Rx 1H Rx endorectal coil in combination with an external multitransmit 1H body array
Hahnemann *et al*[37], 2016	Prospective comparative study	Siemens Terra; custom-built 8-channel Tx/Rx RF body coil with B1+ shimming; coronal bSSFP resolution 0.8mm × 0.8 mm × 2.0 mm, TA = 26s; axial bSSFP, resolution 0.7 mm × 0.7 mm × 2.0 mm, TA = 20s; coronal T2w HASTE, resolution 1.0 mm × 1.0 mm × 5.0 mm, TA = 25s	12	To perform non-enhanced high quality T2w MRI of the small bowel
Gajdošík *et al* [22], 2014	Prospective study	Siemens Terra; 10 cm diameter Tx/Rx surface coil (Rapid Biomedical GmbH, Rimpar, Germany); STEAM sequence; resolution 30 mm × 30 mm × 30 mm	11	To assess the proton T1 and T2 relaxation of *in vivo* hepatic water, choline and lipid metabolites with possible J-coupling behavior of lipids in healthy volunteers
Pang *et al*[15], 2011	Pilot study	bisected microstrip transceiver surface coil; SSFP sequence; TA < 20s	-	For liver imaging

Cervelli *et al* [23], 2022	Feasibility study (*ex-vivo*)	GE Signa; 8-channel Tx/Rx knee RF coil; morphologic sequences: 3D-T2w-CUBE, IDEAL T1w and T2w, 2D- and 3D-MRCP; Quantitative sequences: MP2-RAGE, MSE, IDEAL, 2D-MRF	N/A	For differentiating between tumour and non-target pancreatic tissue using conventional T1w-, T2w- sequences and MRF-derived relaxometry. The MRF sequence obtained reliable relaxation time data
Umutlu *et al* [24], 2011	Prospective study	Siemens Terra; a custom-built 8-channel Tx/Rx RF body coil; 2D FLASH, resolution = 0.8 mm × 0.8 mm × 2.0 mm, TA = 31s; 3D FLASH, resolution 1.3 mm × 1.3 mm × 1.6 mm, TA = 27s; IP and O/P GRE, resolution 1.1 mm × 1.1 mm × 3 .0 mm, TA = 20s; bSSFP, resolution 1.3 mm × 1.6 mm × 4.0 mm, TA = 19s; T2w TSE, resolution 1.4 mm × 1.4 mm × 5.5 mm, TA = 34s	8	For renal imaging
Umutlu *et al* [25], 2011	Prospective study	Siemens Terra; custom-built body Tx/Rx RF coil; T2w BSSFP, resolution 1.3 mm × 1.6 mm × 4.0 mm; T2w TSE; I/P and O/PGRE; T1w 2D FLASH, resolution 0.8 mm × 0.8 mm × 2.0 mm	10	To assess the feasibility of dynamic CE renal imaging
Umutlu *et al* [26], 2012	Prospective study	Siemens Terra; custom-built Tx/Rx RF body array coil; Coronal Fat-Saturated 2D FLASH , TA = 31s; Coronal Fat-Saturated 3D FLASH TA = 27s; Axial Fat-Saturated 2D TOF MRA TA = 33s	12	To investigate the feasibility of 7T nonenhanced high-field MRA of the renal vasculature and to evaluate the diagnostic potential of various non-enhanced T1-weighted spoiled gradient-echo sequences
Laader *et al* [29], 2018	Prospective study	Siemens Terra; custom-built eight-channel Tx/Rx RF body coil; axial 2D T1w TOF MRA TA = 33s; Coronal fat-saturated 3D low-dose CE T1w FLASH VIBE, TA = 27s	10	To evaluate the performance of time-of-flight MRA versus low-dose CE renal MRA at 7T in order to reduce and/or completely omit contrast agent use for renal MRA at 7T
Umutlu *et al* [27], 2013	Prospective study	Siemens Terra; custom-built Tx/Rx RF coil; coronal T1w3D FLASH sequence	8	To assess the feasibility of first-pass CE renal MRA at 7T

TR: Relaxation time; TE: Echo time; TA: Acquisition time; RF: Radiofrequency; T1w: T1 relaxation-weighting; T2w: T2 relaxation-weighting; TOF: Time-of-flight; MRA: Magnetic resonance angiography; CSI: Chemical shift imaging; MRSI: Magnetic resonance spectroscopic imaging; MSE: Multiple spin echo; MRF: Magnetic resonance fingerprinting; MP2RAGE: Magnetization-prepared 2 rapid acquisition gradient echo; MRCP: Magnetic resonance cholangiopancreatography; UTE: Ultrashort echo time; CE: Contrast-enhanced; FLASH: Fast low angle shot magnetic resonance imaging; FSE: Fast spin echo; TSE: Turbo spin echo; DWI: Diffusion weighted imaging; EPI: Echo planar imaging; HASTE: Half fourier single-shot turbo spin-echo; SSFP: Steady-state free precession MRI; N/A: Not applicable.

DISCUSSION

Evaluation of liver and hepatobiliary diseases

The advancements in shimming of the B1 field generated by the 7T multi-channel transmit/receive radiofrequency (RF) body coil has created a foundation for effectively applying 7T MRI in abdominal imaging. Numerous studies have reviewed the progress in high field imaging ranging from non-enhanced MR angiography (MRA) studies to the use of magnetic resonance spectroscopy (MRS) for the detection of metabolic alterations associated with liver diseases including non-alcoholic fatty liver disease (NAFLD), non-alcoholic steatohepatitis (NASH), and cirrhosis, emphasizing the inherent ability of 7T to improve the signal-to-noise ratio (SNR) in various anatomical regions[13,14]. Liver imaging at 7T is particularly interesting due to the expected improvements in SNR, and short echo times can enable the acquisition of high-resolution images (in particular in T1w sequences) with reduced motion artifacts. The susceptibility effect is also more prominent at higher field strengths, where 7T susceptibility-weighted imaging has demonstrated enhanced detection and quantification of hepatic iron stores[15].

Despite these advantages, there exist technical challenges in transferring liver imaging protocols to high magnetic field scanners, specifically related to RF coil and sequence design. For example, a finite-difference time-domain method has been employed to analyse RF field penetration behaviour at 7T, revealing limitations in imaging coverage and RF penetration in human liver imaging at 7T[15]. Elliptically-shaped tissues like the brain may experience a dielectric effect where the short RF wavelength at 7T couples with tissue and forms standing waves, yielding increased B1 penetration and inhomogeneity due to enhanced constructive and destructive interference respectively[16]. The irregular geometry of the liver may limit this effect, leading to reduced B1 penetration and image coverage. To overcome this limitation, a large-sized microstrip transceiver coil for deeper penetration in liver imaging was proposed. On the other hand, a benefit of lessened dielectric effect in the liver is lessened dielectric shading artifacts.

Non-enhanced T1w imaging, [especially time-of-flight magnetic resonance angiography (TOF-MRA)] holds promise for high-quality liver vessel assessment at 7T, offering sharply defined vessel signals and effective background signal suppression with successful visualization of intracranial, renal, and lower extremity vessels. Despite the longer examination time for TOF-MRA, Fischer *et al*[17] highlighted its advantages in delineating three types of liver vessels: the right portal vein, the inferior vena cava and the middle hepatic vein. It was shown that compared to non-enhanced T1w 2D FLASH and T1w 3D FLASH sequences, TOF-MRA has high overall image quality and vessel delineation showing significantly higher contrast ratios for all liver vessels, with the least impairment by B1 inhomogeneity and susceptibility artifacts.

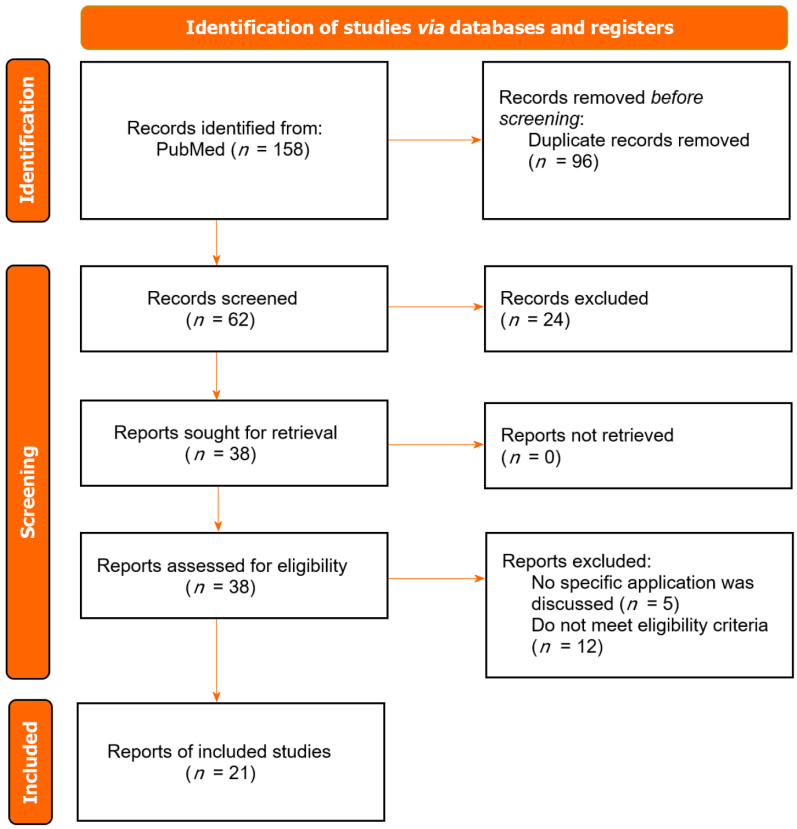

DOI: 10.4329/wjr.v16.i1.20

Figure 1 Flow diagram of the study selection[10].

Both steady-state free precession (SSFP), the most common technique for non-enhanced MR angiography, and T2-weighted (T2W) turbo spin echo (TSE) imaging techniques face limitations in non-contrast-enhanced liver vessel imaging at 7T. SSFP imaging is susceptible to signal heterogeneity in the static magnetic field B0, leading to signal loss artifacts. Additionally, SSFP sequences at 7T encounter challenges related to specific absorption rate (SAR) limitations, with SAR increasing with the square of the magnetic field and the flip angle, potentially constraining usable flip angles such that image signal is inadequate. T2W TSE imaging is also challenging at higher field strengths, since B1 field inhomogeneity and constraints in available RF power for generating accurate refocusing pulses and high flip angles can limit the efficacy of this sequence at higher magnetic field strengths. Consequently, exploiting the inherently hyperintense vessel signal in T1w MRI could be a more promising approach for non-contrast-enhanced liver vessel imaging at 7T[17].

MRS at 7T has been noted for its potential clinical applicability stemming from the high spectral resolution and SNR achieved in a tertiary (research) setting. Studies have highlighted the limitations of liver biopsy as the reference standard for diagnosing NASH, and there has been a focus on the need for non-invasive tools to monitor the severity and progression of NAFLD[18,19]. As a result, proton (1H)- and phosphorus (31P)-MRS have been considered potential candidates for real-time detection of hepatic fat, cell membrane, and energy metabolism. While 3T 1H-MRS is effective for quantifying liver steatosis, a study by Traussnigg *et al*[20] additionally studied the clinical potential of 7T 31P-MRS in NAFLD patients[8]. Their study sought to obtain novel mechanistic insights into lipid, cell membrane, and energy homeostasis in NAFLD by leveraging the increased SNR and spectral resolution of 7T 31P-MRS. The study performed a retrospective analysis of spectra acquired from young healthy volunteers, which indicated a statistical increase in phosphocreatine (PCr) to total phosphorus signal from the liver of patients with advanced fibrosis. The presence of PCr signals in NAFLD or diabetes patients has not been shown in previous studies[20]. The study acknowledged some technical limitations, such as the limited transmit bandwidth restricting effective excitation of β-ATP signal at 7T. Nevertheless, 7T 31P-MRS could be considered a highly accurate and fast non-invasive method for generating comprehensive *in vivo* profiles of lipid, cell membrane, and energy metabolism in the human liver. The findings indicate significant differences in hepatic energy metabolism between NAFL and NASH, providing valuable insights for further mechanistic and therapeutic studies of NAFLD/NASH[20].

Similarly, in the same year another study explored the utility of 7T 31P spectroscopy for investigating liver metabolism, providing novel insights by measuring T1 values for key metabolites like phosphatidylcholine (PtdC), phosphoenolpyruvate (PEP), nicotinamide adenine dinucleotide (NAD+), and uridine diphosphoglucose (UDPG). Chemical Shift Imaging (CSI) was employed with a receive array that achieved approximately 46% coverage of the liver to localize spectra from a specific volume[21]. The study validated the protocol's accuracy and repeatability in both healthy volunteers and cirrhosis patients, demonstrating significant differences in metabolites such as inorganic phosphate (Pi), PEP/PtdC, and glycerophosphoetanolamine. Notably, the study reported a 12% reduction in Pi in cirrhosis patients, indicating the potential of 7T 31P spectroscopy to detect metabolic alterations associated with liver diseases. They

DOI: 10.4329/wjr.v16.i1.20 **Copyright** ©The Author(s) 2024.

Figure 2 Risk of bias associated with the studies included in the review.

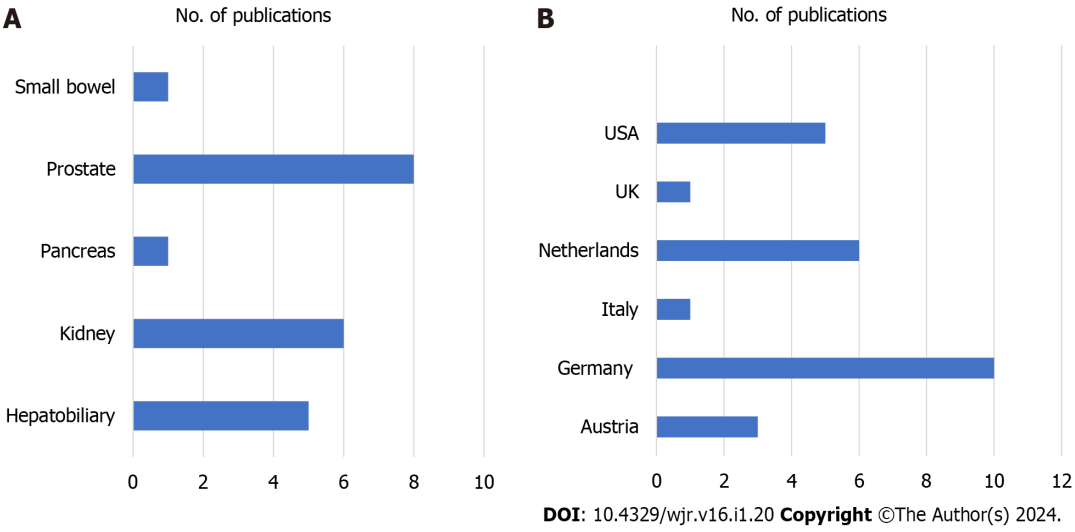

DOI: 10.4329/wjr.v16.i1.20 **Copyright** ©The Author(s) 2024.

Figure 3 Charts illustrating the distribution of clinical 7T abdominal imaging studies. A: Organ system; B: Country.

concluded that 7T 31P spectroscopy is a powerful and reliable tool for in-depth investigations into liver metabolism, offering valuable insights into T1 relaxation times and metabolic changes associated with cirrhosis[21].

Lastly, Gajdošík *et al*[22] delved into the 1H magnetic resonance relaxation behaviour within hepatic tissue at 7T. In vivo T1 and T2 relaxation times for water, methyl groups, and various lipids were quantified. The study successfully resolved key metabolites and maintained a well-tolerated protocol within a 60-min timeframe for volunteers. The findings highlight the potential for future applications in characterizing diverse liver pathologies.

Assessment of pancreatic diseases

For what concerns the pancreas, the aim of 7T MRI so far has been to identify useful imaging biomarkers by evaluating the radiological-histopathological correlation of pancreatic lesions. A recent study[23] evaluated the correlation between 7T MRI findings and histological features in Pancreatic Ductal Adenocarcinoma (PDAC) lesions, with a secondary endpoint of identifying useful MR quantitative sequences for defining an optimal acquisition protocol. MRI findings were compared with the histological composition of *ex-vivo* specimens from lesions preoperatively diagnosed as PDAC *via* computed tomography scan, where *ex-vivo* samples were chosen to overcome limitations of the study[23]. Despite careful coregistration of 7T MRI data with macroscopic and microscopic histological evaluations of pancreaticobiliary lesions, this feat was challenged by a lack of sample uniformity in tumour histology. The results demonstrated the utility of Magnetization Prepared 2 Rapid Acquisition Gradient Echo (MP2RAGE), multiple spin-echo (MSE), and magnetic resonance fingerprinting (MRF)-derived relaxometry in distinguishing tumoral regions from unaffected pancreatic tissue, with MRF demonstrating the capacity for obtaining reliable relaxation time data within a breath hold. Yet, further exploration is needed to understand MRF's role in differentiating the pancreaticobiliary lesion, peritumoral stroma, and residual pancreatic gland. The study concluded that with further validation MRF could play a valuable role in the imaging evaluation of pancreatic tumours[23].

Evaluation of renal and adrenal diseases

Some studies conducted a series of renal imaging studies at 7T. Initial studies were feasibility studies while subsequent studies compared different imaging sequences for their ability to obtain high quality images by reducing or avoiding the use of contrast[24-27].

Initially, they successfully performed renal 7T MRI in eight subjects, with the T1w GRE sequence delivering high anatomical detail and excellent visibility of non-enhanced vasculature, and B1 shimming able to reduce signal voids in most sequence types. Nevertheless, the study suffered from B0 and B1 inhomogeneities (especially in T2w TSE sequences), chemical shift artifacts, RF wavelength effects, and specific absorption rate (SAR) limitations. Despite these difficulties, all 7T examinations were well-tolerated by subjects with an average examination time of 25 min[24]. In the same year, the same group assessed the feasibility of intravenous injection of Gadobutrol for dynamic contrast-enhanced renal MRI at 7T in ten healthy subjects. Among the sequences tested, T1w 2D FLASH yielded the best overall image quality, while T2w TSE had the poorest image quality. Additionally, quantitative analysis highlighted the advantages of arterial phase 3D FLASH imaging in terms of contrast to noise (CNR) between cortex and medulla[25].

In the following year, the same researchers explored the feasibility of non-enhanced 7T MRA for assessing renal perfusion and to evaluate renal vasculature using various T1w sequences. The study also addressed safety concerns related to Gadolinium-based contrast agents and their link to nephrogenic systemic fibrosis. Initial results demonstrated the feasibility and challenges of non-enhanced 7T renal MRA, ultimately emphasizing the superiority of TOF imaging in the tested sequences[26]. Shortly thereafter, they evaluated first-pass contrast-enhanced renal 7T MRA. Eight healthy subjects underwent dynamic imaging with contrast, resulting in high definition of the arterial vasculature and increased SNR and CNR upon administration of contrast. The study concluded that first-pass contrast-enhanced renal 7T MRA is technically feasible and provides superior vessel assessment compared to non-enhanced MRA[27]. Finally, they explored the viability of reducing 7T MRA renal Gadobutrol dosage in ten healthy volunteers, and showed that a reduced dose of 0.025 mmol/kg body weight can maintain sufficient image quality[28].

Another study comparing non-enhanced TOF MRA and low-dose contrast-enhanced renal MRA at 7T showed that both methods exhibited moderate overall image quality, with TOF MRA demonstrating less artifacts and better delineation of segmental branches within the renal parenchyma[29]. This indicates the feasibility of reducing or eliminating contrast agents for renal 7T MRA, with a call for further research to validate these findings.

Overall, despite the demonstrated feasibility of various 7T MRI sequences for kidney imaging, several challenges persist. SAR limitations may require sacrifices that include long imaging times and spurious artifacts, especially in T2w sequences; these may be partially addressed with parallel imaging and high amplitude stimulated echoes, which unfortunately may compromise SNR. RF inhomogeneity may be managed through RF shimming, an area of ongoing advancement. T1w sequences at 7T often achieve only comparable results to 3T imaging. Non-contrast-enhanced sequences show promise for renal vascular imaging at 7T, although there are few direct comparisons with contrast-enhanced methods. Despite challenges, the future of renal 7T MRI appears promising.

Evaluation of the prostate

In the context of prostate imaging, 7T MRI has been investigated for the possibility of identifying imaging biomarkers of prostate cancer using different enhanced and non-enhanced sequences. In addition, MRS has been extensively investigated for its accuracy in evaluating metabolomic profiles in prostate cancer, and feasibility studies have been conducted for combined 1H and 31P MRS and related endorectal coils. One of the first reported prostate studies employing 7T MRI evaluated the feasibility of applying metabolomic profiles obtained from intact-tissue 14T MRS to the imaging of whole prostates using multi-voxel 7T MRS. Cancerous samples could be differentiated from histologically benign ones using the

metabolic profile with an overall accuracy of 93%, demonstrating that metabolomic profiles at ultra-high fields could be translated for use in real-world clinical settings[30].

A prostate feasibility study in 2014 by Vos *et al*[31] demonstrated that 7T T2w imaging could employ dedicated multi-transmit RF coils with shimming and SAR-monitoring to generate good image quality. All 17 patients completed the protocol without adverse incident to yield image quality rated as satisfactory by one reader (R1) and good by the other two readers (R2 and R3), with moderate agreement ($\alpha = 0.44$) amongst them. Lesions were successfully visualized in all 7 patients with confirmed prostate cancer. Moderate motion artifacts were observed, and six lesions with low Gleason scores or small volume were not recognized, highlighting the need for future investigations into the impact of the absence of lipid signal at 7T on the detection of extracapsular extension of prostate cancer into periprostatic tissue[31].

That year another study by Luttje *et al*[32] demonstrated the feasibility of combining 7T 1H MRSI and 31P MRSI in the human prostate. The researchers used a customized endorectal coil (ERC) matched and tuned to both 1H and 31P without significant efficiency losses or sensitivity discrepancies between channels. 1H MRSI revealed distinct resonances of choline, polyamines, creatine, and citrate, offering the potential for individual fitting and increased sensitivity in detecting elevated choline levels. They proposed the use of adiabatic RF pulses and coil hardware combinations to combat residual B1+ nonuniformity. In vivo 31P MRSI measurements identified signals of phospholipid metabolites, and contrary to previous findings indicated lower levels of phosphoethanolamine in tumor areas compared to healthy tissue. Combining 1H and 31P MRSI in the same scan session potentially improved diagnostic sensitivity by correlating individual compounds of the choline pool with tumor aggressiveness[32]. Another similar study evaluated safety concerns of a similar 31P/1H ERC in terms of its proximity to tissue. Electromagnetic field simulations and phantom experiments indicated an absence of significant coupling between the 1H and 31P ERC channels and the external body array, with SAR and temperature simulations/measurements confirming procedural safety. Successful application of the 31P/1H ERC in volunteer and patient measurements demonstrated the feasibility and safety for clinical use of 7T prostate imaging and spectroscopy[33].

Other 7T MRSI work in the prostate has been performed, including a study by Lagemaat *et al*[34] aimed at characterization of vivo 31P MR spectra. They assessed T1 relaxation times and the nuclear overhauser effect (NOE) of phosphorus-containing metabolites, and determined that the NOE enhanced fitting accuracy with some variability, and that reducing flip angle (≤ 45°) enabled optimal acquisition in 15 min. Another study used MRSI to discern and localize prostate cancer through distinct choline and citrate signal patterns. Tailored coil designs to address B1+ inhomogeneities and chemical shift artifacts permitted 31P 7T MRSI to enable identification of phosphorus-containing metabolites. Overall insights into prostate tissue biochemistry could be gleaned clinically by leveraging the high 7T SNR to execute 3D 31P MRSI within a clinically acceptable timeframe[12].

Other studies included a two patient 7T T2w TSE MRI analysis using a two-loop transmit system that revealed a focal region of decreased T2 signal in the peripheral zone suspicious for tumors in both patients[35]. Post-prostatectomy analysis of the specimens confirmed good correspondence between these findings and histopathologic assessment of the dominant peripheral zone tumor[35]. Another study by Durand *et al*[36] sought to balance 7T resolution and scan time to image the prostate gland. High resolution 100 μm × 107 μm × 750 μm (11 min) and 60 μm × 60 μm × 90 μm (3 h) protocols allowed visualization of prostatic microanatomy, aiding in distinguishing benign and malignant tissues, including adenocarcinomas with Gleason scores of 7, 8, and 9. The study suggests that these images could serve as a diagnostic non-invasive alternative to biopsy, and improve treatment planning precision through accurate tumor volume estimation[36].

Finally, there have been indications of other potential clinical applications of 7T MRI in prostate imaging. Dynamic contrast-enhanced MRI (DCE MRI) at 7T is a promising method due to the possibility of enhanced spatial and temporal resolution, vital for precise pharmacokinetic modeling and qualitative assessment in prostate cancer detection. The R2* relaxation rate using Gadolinium-based contrast agents purportedly quadruples at 7T relative to 3T, significantly impacting DCE-MRI signal, especially in blood[12]. 7T MRI also holds promise for detecting lymph node metastases in prostate cancer patients, offering enhanced spatial resolution for visualizing nodes smaller than 5 mm. Functional MRI contrast agents such as ferumoxtran-10 may aid in distinguishing between normal and metastatic lymph nodes, although efforts in this capacity have thus far been limited to clinical trials[12].

Evaluation of the small bowel

As of the writing of this article, there does not seem to be any significant advantage to imaging the small bowel at 7T relative to traditional MRI field strengths. A study by Hahnemann *et al* assessed the feasibility and efficacy of non-enhanced small bowel MRI at both 1.5 T and 7T using fast imaging with balanced steady-state free precession (bSSFP) and half-Fourier acquisition single-shot turbo spin-echo sequences[37]. The comparison revealed that mesentery contrast and tissue detail delineation were generally superior and occasionally similar at 1.5T relative to 7T across all subjects. Contrast of the jejunum and ileum were mostly equivalent at 1.5T and 7T, with one subject exhibiting superior contrast of the ileum at 1.5T[37]. Quantitative analysis demonstrated no statistically significant differences in tissue contrast between the bowel wall and lumen for 1.5T and 7T in coronal bSSFP, although some axial images revealed significantly higher contrast at 1.5T. Overwhelming B1 inhomogeneity and susceptibility artifact in 7T bSSFP imaging led the study to conclude that although small bowel MRI at 7T is technically feasible, tissue contrast and image fidelity are at best comparable to that achieved at 1.5 T MRI[37].

Limitations of our analysis

It is essential to recognize several limitations of our systematic review. First, our search of records could have missed some publications indexed in other databases like EMBASE, Scopus, Google scholar, *etc.* However, PubMed is known for its appropriate and high-quality content from peer-reviewed medical journals, which indicates its applicability for

conducting systematic reviews in medicine. Systematic reviews involve a trade-off between comprehensiveness and feasibility, and including too many databases can make processing time unwieldy. Note that a manual search in EMBASE using the same search criteria showed very few missed studies, suggesting that the sacrifice of avoiding its use was relatively small. Second, some areas of study were not adequately represented in the literature, such as imaging of the small bowel and pancreas at 7T. Lastly, a meta-analysis of diagnostic accuracy could not be conducted due to the lack of adequate studies with similar objectives.

CONCLUSION

While 7T MRI demonstrates remarkable imaging potential, the limitations stemming from inhomogeneous excitation fields call for ongoing efforts in optimizing dedicated RF coil and pulse design. Further research and technological advancements are crucial to harness the benefits of high magnetic field strengths while mitigating the challenges associated with these advancements in MRI technology.

ARTICLE HIGHLIGHTS

Research background

Clinical 7-Tesla HASTE was approved for clinical use in 2017. Since then, it has been used widely in specialized research centers mainly for neuroimaging studies. However, it has been also used in the imaging of abdominal organs even though the studies are few.

Research motivation

To summarize all the current evidence concerning the utilization of 7-Tesla MRI in clinical abdominal imaging since to our knowledge there has been no review paper discussing this before.

Research objectives

To offer a comprehensive overview of current literature on clinical abdominal 7T MRI that emphasizes current trends, to summarize the current imaging sequences/parameters used, to describe relevant challenges, and to provide a concise set of potential solutions.

Research methods

This systematic review adheres to PRISMA guidelines. A PubMed search, utilizing Medical Subject Headings terms such as "7-Tesla" and organ-specific terms, was conducted for articles published between January 1, 1985, and July 25, 2023. Eligibility criteria included studies exploring 7T MRI for imaging human abdominal organs, encompassing various study types (*in-vivo*/*ex-vivo*, method development, reviews/meta-analyses). Exclusion criteria involved animal studies and those lacking extractable data. Study selection involved initial identification *via* title/abstract, followed by a full-text review by two researchers, with discrepancies resolved through discussion. Data extraction covered publication details, study design, population, sample size, 7T MRI protocol, image characteristics, endpoints, and conclusions.

Research results

The systematic review encompassed a total of 21 studies. Analysis of the distribution of clinical 7T abdominal imaging studies indicated a predominant emphasis on the prostate (n = 8), followed by the kidney (n = 6), and the hepatobiliary system (n = 5). Research on these organs, as well as the pancreas, demonstrated evident advantages at 7T. Conversely, studies on the small bowel did not reveal significant enhancements compared to traditional MRI at 1.5T. The majority of the evaluated studies originated from Germany (n = 10), followed by the Netherlands (n = 5), the United States (n = 5), Austria (n = 2), the United Kingdom (n = 1), and Italy (n = 1).

Research conclusions

7T MRI showcases remarkable imaging potential, however, the limitations arising from inhomogeneous excitation fields underscore the need for ongoing efforts in optimizing dedicated RF coil and pulse design. Continued research and technological advancements are imperative to fully harness the advantages of high magnetic field strengths while addressing the challenges associated with advancements in MRI technology.

Research perspectives

More studies are necessary to elucidate the full potential of 7-Tesla MRI in abdominal imaging especially when it comes to the imaging of the pancreas, and the intestines which had very few investigative studies.

FOOTNOTES

Author contributions: All authors contributed equally to this work; Perera Molligoda Arachchige AS designed the research study; Perera Molligoda Arachchige AS and Teixeira de Castro Gonçalves Ortega AC performed the research; Catapano F and Politi LS revised the final draft; All authors analyzed the data and wrote the manuscript; Hoff MN supervised the study, revised the final draft; All authors have read and approved the final manuscript.

Conflict-of-interest statement: All the authors have no conflicts of interest to declare.

PRISMA 2009 Checklist statement: The authors have read the PRISMA 2009 Checklist, and the manuscript was prepared and revised according to the PRISMA 2009 Checklist.

Country/Territory of origin: United States

ORCID number: Arosh S Perera Molligoda Arachchige 0000-0002-3875-0267; Letterio S Politi 0000-0002-6190-6688; Michael N Hoff 0000-0002-3498-0591.

S-Editor: Liu JH
L-Editor: A
P-Editor: Zhao S

REFERENCES

1 **Caraiani C**, Yi D, Petresc B, Dietrich C. Indications for abdominal imaging: When and what to choose? *J Ultrason* 2020; **20**: e43-e54 [PMID: 32320166 DOI: 10.15557/JoU.2020.0008]
2 **Harmonay V**. What is the Strongest MRI Machine Today? Atlantis WORLDWIDE. 04th Dec 2023. Available from: https://info.atlantisworldwide.com/blog/what-is-the-strongest-mri-machine
3 **Nowogrodzki A**. The world's strongest MRI machines are pushing human imaging to new limits. *Nature* 2018; **563**: 24-26 [PMID: 30382222 DOI: 10.1038/d41586-018-07182-7]
4 **Arachchige ASPM**. 7-Tesla PET/MRI: A promising tool for multimodal brain imaging? *AIMS Neurosci* 2022; **9**: 516-518 [PMID: 36660074 DOI: 10.3934/Neuroscience.2022029]
5 **Hoff MN**, McKinney A 4th, Shellock FG, Rassner U, Gilk T, Watson RE Jr, Greenberg TD, Froelich J, Kanal E. Safety Considerations of 7-T MRI in Clinical Practice. *Radiology* 2019; **292**: 509-518 [PMID: 31310177 DOI: 10.1148/radiol.2019182742]
6 **Reiter T**, Lohr D, Hock M, Ankenbrand MJ, Stefanescu MR, Kosmala A, Kaspar M, Juchem C, Terekhov M, Schreiber LM. On the way to routine cardiac MRI at 7 Tesla - a pilot study on consecutive 84 examinations. *PLoS One* 2021; **16**: e0252797 [PMID: 34297720 DOI: 10.1371/journal.pone.0252797]
7 **Snyder CJ**, DelaBarre L, Metzger GJ, van de Moortele PF, Akgun C, Ugurbil K, Vaughan JT. Initial results of cardiac imaging at 7 Tesla. *Magn Reson Med* 2009; **61**: 517-524 [PMID: 19097233 DOI: 10.1002/mrm.21895]
8 **Korteweg MA**, Veldhuis WB, Visser F, Luijten PR, Mali WP, van Diest PJ, van den Bosch MA, Klomp DJ. Feasibility of 7 Tesla breast magnetic resonance imaging determination of intrinsic sensitivity and high-resolution magnetic resonance imaging, diffusion-weighted imaging, and (1)H-magnetic resonance spectroscopy of breast cancer patients receiving neoadjuvant therapy. *Invest Radiol* 2011; **46**: 370-376 [PMID: 21317792 DOI: 10.1097/RLI.0b013e31820df706]
9 **Vaughan JT**, Snyder CJ, DelaBarre LJ, Bolan PJ, Tian J, Bolinger L, Adriany G, Andersen P, Strupp J, Ugurbil K. Whole-body imaging at 7T: preliminary results. *Magn Reson Med* 2009; **61**: 244-248 [PMID: 19097214 DOI: 10.1002/mrm.21751]
10 **Page MJ**, McKenzie JE, Bossuyt PM, Boutron I, Hoffmann TC, Mulrow CD, Shamseer L, Tetzlaff JM, Akl EA, Brennan SE, Chou R, Glanville J, Grimshaw JM, Hróbjartsson A, Lalu MM, Li T, Loder EW, Mayo-Wilson E, McDonald S, McGuinness LA, Stewart LA, Thomas J, Tricco AC, Welch VA, Whiting P, Moher D. The PRISMA 2020 statement: an updated guideline for reporting systematic reviews. *BMJ* 2021; **372**: n71 [PMID: 33782057 DOI: 10.1136/bmj.n71]
11 **Sterne JAC**, Savović J, Page MJ, Elbers RG, Blencowe NS, Boutron I, Cates CJ, Cheng HY, Corbett MS, Eldridge SM, Emberson JR, Hernán MA, Hopewell S, Hróbjartsson A, Junqueira DR, Jüni P, Kirkham JJ, Lasserson T, Li T, McAleenan A, Reeves BC, Shepperd S, Shrier I, Stewart LA, Tilling K, White IR, Whiting PF, Higgins JPT. RoB 2: a revised tool for assessing risk of bias in randomised trials. *BMJ* 2019; **366**: l4898 [PMID: 31462531 DOI: 10.1136/bmj.l4898]
12 **Tenbergen CJA**, Metzger GJ, Scheenen TWJ. Ultra-high-field MR in Prostate cancer: Feasibility and Potential. *MAGMA* 2022; **35**: 631-644 [PMID: 35579785 DOI: 10.1007/s10334-022-01013-7]
13 **Verma Y**, Ramesh S, Perera Molligoda Arachchige AS. 7 T Versus 3 T in the Diagnosis of Small Unruptured Intracranial Aneurysms: Reply to Radojewski et al. *Clin Neuroradiol* 2023 [PMID: 37318559 DOI: 10.1007/s00062-023-01321-y]
14 **Trattnig S**, Springer E, Bogner W, Hangel G, Strasser B, Dymerska B, Cardoso PL, Robinson SD. Key clinical benefits of neuroimaging at 7T. *Neuroimage* 2018; **168**: 477-489 [PMID: 27851995 DOI: 10.1016/j.neuroimage.2016.11.031]
15 **Pang Y**, Wu B, Wang C, Vigneron DB, Zhang X. Numerical Analysis of Human Sample Effect on RF Penetration and Liver MR Imaging at Ultrahigh Field. *Concepts Magn Reson Part B Magn Reson Eng* 2011; **39B**: 206-216 [PMID: 22337345 DOI: 10.1002/cmr.b.20209]
16 **Ibrahim TS**, Lee R, Abduljalil AM, Baertlein BA, Robitaille PM. Dielectric resonances and B(1) field inhomogeneity in UHFMRI:

computational analysis and experimental findings. *Magn Reson Imaging* 2001; **19**: 219-226 [PMID: 11358660 DOI: 10.1016/S0730-725X(01)00300-9]

17 **Fischer A**, Kraff O, Maderwald S, Beiderwellen K, Ladd ME, Forsting M, Lauenstein TC, Umutlu L. Non-enhanced T1-weighted liver vessel imaging at 7 Tesla. *PLoS One* 2014; **9**: e97465 [PMID: 24887206 DOI: 10.1371/journal.pone.0097465]

18 **Sumida Y**, Nakajima A, Itoh Y. Limitations of liver biopsy and non-invasive diagnostic tests for the diagnosis of nonalcoholic fatty liver disease/nonalcoholic steatohepatitis. *World J Gastroenterol* 2014; **20**: 475-485 [PMID: 24574716 DOI: 10.3748/wjg.v20.i2.475]

19 **Tincopa MA**, Loomba R. Non-invasive diagnosis and monitoring of non-alcoholic fatty liver disease and non-alcoholic steatohepatitis. *Lancet Gastroenterol Hepatol* 2023; **8**: 660-670 [PMID: 37060912 DOI: 10.1016/S2468-1253(23)00066-3]

20 **Traussnigg S**, Kienbacher C, Gajdošík M, Valkovič L, Halilbasic E, Stift J, Rechling C, Hofer H, Steindl-Munda P, Ferenci P, Wrba F, Trattnig S, Kršňák M, Trauner M. Ultra-high-field magnetic resonance spectroscopy in non-alcoholic fatty liver disease: Novel mechanistic and diagnostic insights of energy metabolism in non-alcoholic steatohepatitis and advanced fibrosis. *Liver Int* 2017; **37**: 1544-1553 [PMID: 28544208 DOI: 10.1111/liv.13451]

21 **Purvis LAB**, Clarke WT, Valkovič L, Levick C, Pavlides M, Barnes E, Cobbold JF, Robson MD, Rodgers CT. Phosphodiester content measured in human liver by in vivo (31) P MR spectroscopy at 7 tesla. *Magn Reson Med* 2017; **78**: 2095-2105 [PMID: 28244131 DOI: 10.1002/mrm.26635]

22 **Gajdošík M**, Chmelík M, Just-Kukurová I, Bogner W, Valkovič L, Trattnig S, Kršňák M. In vivo relaxation behavior of liver compounds at 7 Tesla, measured by single-voxel proton MR spectroscopy. *J Magn Reson Imaging* 2014; **40**: 1365-1374 [PMID: 24222653 DOI: 10.1002/jmri.24489]

23 **Cervelli R**, Cencini M, Cacciato Insilla A, Aringhieri G, Boggi U, Campani D, Tosetti M, Crocetti L. Ex-vivo human pancreatic specimen evaluation by 7 Tesla MRI: a prospective radiological-pathological correlation study. *Radiol Med* 2022; **127**: 950-959 [PMID: 35984559 DOI: 10.1007/s11547-022-01533-1]

24 **Umutlu L**, Orzada S, Kinner S, Maderwald S, Brote I, Bitz AK, Kraff O, Ladd SC, Antoch G, Ladd ME, Quick HH, Lauenstein TC. Renal imaging at 7 Tesla: preliminary results. *Eur Radiol* 2011; **21**: 841-849 [PMID: 20872006 DOI: 10.1007/s00330-010-1962-9]

25 **Umutlu L**, Kraff O, Orzada S, Fischer A, Kinner S, Maderwald S, Antoch G, Quick HH, Forsting M, Ladd ME, Lauenstein TC. Dynamic contrast-enhanced renal MRI at 7 Tesla: preliminary results. *Invest Radiol* 2011; **46**: 425-433 [PMID: 21317791 DOI: 10.1097/RLI.0b013e31820e1467]

26 **Umutlu L**, Maderwald S, Kraff O, Kinner S, Schaefer LC, Wrede K, Antoch G, Forsting M, Ladd ME, Lauenstein TC, Quick HH. New look at renal vasculature: 7 tesla nonenhanced T1-weighted FLASH imaging. *J Magn Reson Imaging* 2012; **36**: 714-721 [PMID: 22649028 DOI: 10.1002/jmri.23702]

27 **Umutlu L**, Maderwald S, Kinner S, Kraff O, Bitz AK, Orzada S, Johst S, Wrede K, Forsting M, Ladd ME, Lauenstein TC, Quick HH. First-pass contrast-enhanced renal MRA at 7 Tesla: initial results. *Eur Radiol* 2013; **23**: 1059-1066 [PMID: 23064714 DOI: 10.1007/s00330-012-2666-0]

28 **Beiderwellen K**, Kraff O, Laader A, Maderwald S, Orzada S, Ladd ME, Forsting M, Lauenstein TC, Umutlu L. Contrast enhanced renal MR angiography at 7 Tesla: How much gadolinium do we need? *Eur J Radiol* 2017; **86**: 76-82 [PMID: 28027770 DOI: 10.1016/j.ejrad.2016.11.007]

29 **Laader A**, Beiderwellen K, Kraff O, Maderwald S, Ladd ME, Forsting M, Umutlu L. Non-enhanced versus low-dose contrast-enhanced renal magnetic resonance angiography at 7 T: a feasibility study. *Acta Radiol* 2018; **59**: 296-304 [PMID: 28691526 DOI: 10.1177/0284185117718399]

30 **Wu CL**, Jordan KW, Ratai EM, Sheng J, Adkins CB, Defeo EM, Jenkins BG, Ying L, McDougal WS, Cheng LL. Metabolomic imaging for human prostate cancer detection. *Sci Transl Med* 2010; **2**: 16ra8 [PMID: 20371475 DOI: 10.1126/scitranslmed.3000513]

31 **Vos EK**, Lagemaat MW, Barentsz JO, Fütterer JJ, Zámecnik P, Roozen H, Orzada S, Bitz AK, Maas MC, Scheenen TW. Image quality and cancer visibility of T2-weighted magnetic resonance imaging of the prostate at 7 Tesla. *Eur Radiol* 2014; **24**: 1950-1958 [PMID: 24865699 DOI: 10.1007/s00330-014-3234-6]

32 **Luttje MP**, Italiaander MG, Arteaga de Castro CS, van der Kemp WJ, Luijten PR, van Vulpen M, van der Heide UA, Klomp DW. (31) P MR spectroscopic imaging combined with (1) H MR spectroscopic imaging in the human prostate using a double tuned endorectal coil at 7T. *Magn Reson Med* 2014; **72**: 1516-1521 [PMID: 24357271 DOI: 10.1002/mrm.25070]

33 **Philips BWJ**, van Uden MJ, Rietsch SHG, Orzada S, Scheenen TWJ. A multitransmit external body array combined with a (1) H and (31) P endorectal coil to enable a multiparametric and multimetabolic MRI examination of the prostate at 7T. Med Phys 2019; 46: 3893-3905 [PMID: 31274201 DOI: 10.1002/mp.13696]

34 **Lagemaat MW**, Maas MC, Vos EK, Bitz AK, Orzada S, Weiland E, van Uden MJ, Kobus T, Heerschap A, Scheenen TW. (31) P MR spectroscopic imaging of the human prostate at 7 T: T1 relaxation times, Nuclear Overhauser Effect, and spectral characterization. Magn Reson Med 2015; 73: 909-920 [PMID: 24677408 DOI: 10.1002/mrm.25209]

35 **Rosenkrantz AB**, Zhang B, Ben-Eliezer N, Le Nobin J, Melamed J, Deng FM, Taneja SS, Wiggins GC. T2-weighted prostate MRI at 7 Tesla using a simplified external transmit-receive coil array: correlation with radical prostatectomy findings in two prostate cancer patients. J Magn Reson Imaging 2015; 41: 226-232 [PMID: 24259458 DOI: 10.1002/jmri.24511]

36 **Durand M**, Jain M, Robinson B, Aronowitz E, El Douahy Y, Leung R, Scherr DS, Ng A, Donzeau D, Amiel J, Spincemaille P, Villers A, Ballon DJ. Magnetic resonance microscopy may enable distinction between normal histomorphological features and prostate cancer in the resected prostate gland. BJU Int 2017; 119: 414-423 [PMID: 27154761 DOI: 10.1111/bju.13523]

37 **Hahnemann ML**, Kraff O, Maderwald S, Johst S, Orzada S, Umutlu L, Ladd ME, Quick HH, Lauenstein TC. Non-enhanced magnetic resonance imaging of the small bowel at 7 Tesla in comparison to 1.5 Tesla: First steps towards clinical application. *Magn Reson Imaging* 2016; **34**: 668-673 [PMID: 26747410 DOI: 10.1016/j.mri.2015.11.012]

Published by **Baishideng Publishing Group Inc**
7041 Koll Center Parkway, Suite 160, Pleasanton, CA 94566, USA
Telephone: +1-925-3991568
E-mail: office@baishideng.com
Help Desk: https://www.f6publishing.com/helpdesk
https://www.wjgnet.com